Forschungszentrum Karlsruhe
Technik und Umwelt

Wissenschaftliche Berichte
FZKA 5517

Thermohydraulic Performances of the Cable-in-conduit Conductor for the Wendelstein 7-X Magnet System

X. Cheng, W. Lehmann

Institut für Technische Physik
Projekt Kernfusion

Februar 1995

Forschungszentrum Karlsruhe
Technik und Umwelt
Wissenschaftliche Berichte
FZKA 5517

Thermohydraulic Performances of the Cable-in-conduit Conductor for the Wendelstein 7-X Magnet System

X. Cheng*), W. Lehmann

Institut für Technische Physik
Projekt Kernfusion

*) Present address: Institut für Strömungslehre und Strömungsmaschinen
Technische Universität Karlsruhe

Forschungszentrum Karlsruhe GmbH, Karlsruhe
1995

Als Manuskript gedruckt

Forschungszentrum Karlsruhe GmbH
Postfach 3640, 76021 Karlsruhe

ISSN 0947-8620

Thermohydraulic performances of the cable-in-conduit conductor for the Wendelstein 7-X magnet system

Abstract

Experimental investigations were performed on pressure drop and transversal heat transfer in the cable-in-conduit conductor (CICC) for the Wendelstein 7-X magnet system. For this purpose the HELITEX test facility of KfK/ITP has been used. To evaluate the experimental results of the transversal heat transfer, a theoretical method was developed which could also be applied to other types of superconductors.

The friction factor measured in the W7-X conductors is roughly three times the values in an equivalent smooth circular channel and can be well reproduced by a modified Prandtl-Karman equation.

Experimental results emphasize that the transversal heat transfer between flow channel and jacket can not be described accurately either by pure heat conduction or by pure heat convection. Based on a physical mechanism, a new model was developed which considers heat conduction and heat convection simultaneously and is also applicable to other CICC's. For the W7-X conductor used equations of transversal heat transfer were derived.

The thermal conductivity of the insulating layer measured in two test sections with different values of layer thickness agrees well with each other. It increases with increasing temperature and shows satisfying agreement with the data given in the literature.

Thermohydraulische Eigenschaften des Wendelstein 7-X-Leiters

Kurzfassung

Experimentelle Untersuchungen zum Druckverlust und transversalen Wärmeübergang im W7-X-Leiter wurden in der HELITEX-Anlage des KfK/ITP durchgeführt. Außerdem wurde eine theoretische Methode zur Auswertung der Versuchsergebnisse entwickelt. Diese Methode kann auch auf andere Typen von Leitern angewandt werden.

Der gemessene Reibungsbeiwert ist etwa dreifach im Vergleich zum glatten Rohr. Die Meßdaten können mit einer modifizierten Prandtl-Karman-Gleichung sehr gut wiedergegeben werden.

Es wurde festgestellt, daß der transversale Wärmeübergang zwischen dem Strömungskanal und dem Gehäuse weder durch reine Wärmeleitung noch durch rein konvektiven Wärmeübergang ausreichend genau beschrieben werden kann. Daher wurde ein physikalisches Modell entwickelt, das die Wärmeleitung und den konvektiven Wärmeübergang gleichzeitig berücksichtigt. Das Modell ist allgemein gültig für die Leiter des CICC-Typs. Anhand von Meßergebnissen wurden Gleichungen abgeleitet, die den transversalen Wärmeübergang in den W7-X-Leiter beschreiben.

Die Wärmeleitfähigkeit der Isolationsschicht, gemessen auf zwei Teststrecken mit unterschiedlichen Dicken der Isolationsschicht, stimmen gut miteinander überein. Die gemessene Wärmeleitfähigkeit nimmt mit erhöhter Temperatur zu und zeigt qualitativ eine gute Übereinstimmung mit den in der Literatur angegebenen Werten.

Contents

1. Introduction ... 1

2. Experimental apparatus ... 3

2.1 Helitex test facility ... 3
2.2 Test sections ... 5
2.3 Test matrix ... 8
2.4 Measurements ... 9

3. Experimental results and discussion ... 14
3.1 Pressure drop ... 14
3.2 Heat transfer between flow channel and jacket ... 17
3.2.1 Theoretical method of evaluating the transversal heat transfer coefficient ... 17
3.2.1.1 General problem ... 17
3.2.1.2 Heat conduction perpendicular to the flow direction ... 19
3.2.1.3 Heat conduction parallel to the flow direction ... 22
3.2.1.4 Calculation procedure ... 24
3.2.2 Experimental results ... 27
3.2.3 A new model for transversal heat transfer in CICC's ... 29
3.3 Heat conduction through the insulating layer ... 32

4. Conclusions ... 36

References ... 37

Appendix A: THECON - A computer code for two-dimensional heat conduction ... 38

Appendix B: Test results of pressure drop ... 44

Appendix C: Test results of transversal heat transfer between flow channel and jacket ... 51

Appendix D: Test results of thermal conductivity of insulating layers ... 56

1. Introduction

The superconducting magnets for modular stellarator reactors [1] and for the ITER Tokamak reactor [2] use helium forced-flow-cooled, cable-in-conduit conductors (CICC). These conductors are made by winding one over another superconducting wire strands to form a cable. The wound cable is enclosed in a conduit (jacket) to form a cable-in-conduit conductor. The forced-flow supercritical helium flows inside the conduit and cools the cable as well as the jacket. In a magnet system a lot of such conductors are arranged close to each other. Figure 1 shows the cross section of a proposed Wendelstein 7-X (W7-X) coil with 16 conductors. The cable is made of NbTi superconducting wire strands, 0.55 mm in diameter, which is twisted into a 3x4x4x4 geometry. The jacket made of aluminium alloy has a square cross-section (14.8x14.8 mm) with rounded corners. Between neighbouring conductors, insulating layers exist which are made from glass epoxy resin.

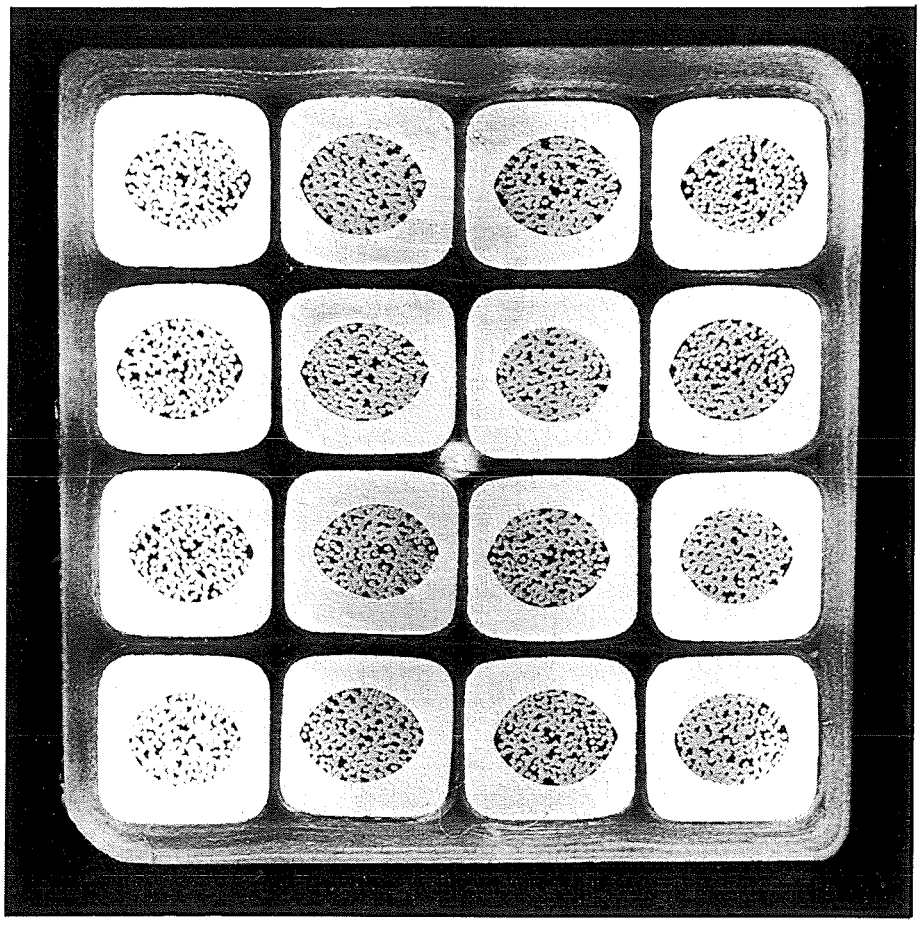

Fig.1: Cross section of a proposed Wendelstein 7-X coil

In case that the wire strands in one of the conductors experience a transition from superconducting to normal conducting state, the temperature of the flow channel (strands plus helium) increases due to the Joule heat released, and transversal heat transfer takes place from the 'hot' flow channel to its 'cold' neighbouring flow channels. The transversal heat transfer can

be divided into three portions, i.e. heat transfer between the flow channel and the jacket, heat conduction through the jacket and heat conduction through the insulating layer.

The thermophysical properties of the jacket are well known. Therefore, heat conduction through the jacket can be easily computed. In contrast, the effective thermal conductivity of the insulating layer is dependent not only on its compositions but also on fabricating procedures. Experimental investigation is necessary to determine exactly the effective thermal conductivity of the insulating layer.

Regarding the transversal heat transfer between the jacket and the flow channel, different methods and correlations are used by different authors, as shown in figure 2.

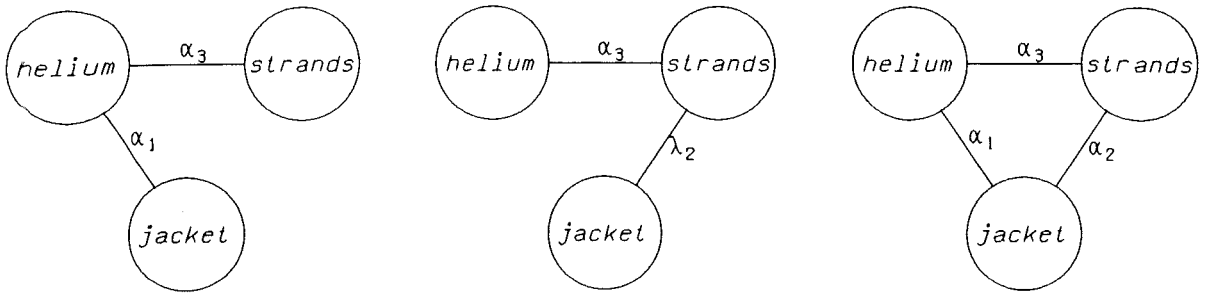

CICC code [3] *MAGS code [4]* *Saruman code [5]*

Fig.2: Models of transversal heat transfer used in different computer codes

Wong [3] neglects the thermal connection between the jacket and the strands. The heat transfer between the jacket and helium is determined by a conventional equation for an equivalent smooth circular channel. Meyder [4] eliminates the convective heat transfer between the jacket and helium. The heat transfer between the jacket and the strands is considered as pure heat conduction. To solve the heat conduction equation, the strands and helium are homogenized to form an equivalent solid material, whose transversal thermal conductivity depends on the composition of the strands as well as on the structure of the flow channel. The equivalent transversal thermal conductivity may be more than thousand times less than the thermal conductivity of the strands itself. Bottura [5] considers separately the heat transfer between the jacket and helium as well as that between the jacket and the strands. Both heat transfer mechanisms are considered as convective ones.

The knowledge of the transversal heat transfer as well as of the pressure drop of the flow within CICC's is important for a safe design of a superconducting magnet system. However, experimentally proved models are not available in the literature up to now, especially concerning the transversal heat transfer. As a consequence, experimental investigations were performed of transversal heat transfer and of pressure drop in conductors for the modular stellarator Wendelstein 7-X (W7-X) magnet system at the Institute of Technical Physics (ITP) of the Nuclear Research Center Karlsruhe (KfK). Additionally, theoretical methods were developed to evaluate the experimental results.

2. Experimental apparatus

2.1 Helitex test facility

The experiment was performed in the **HELITEX** test facility of KfK/ITP (Fig. 3).

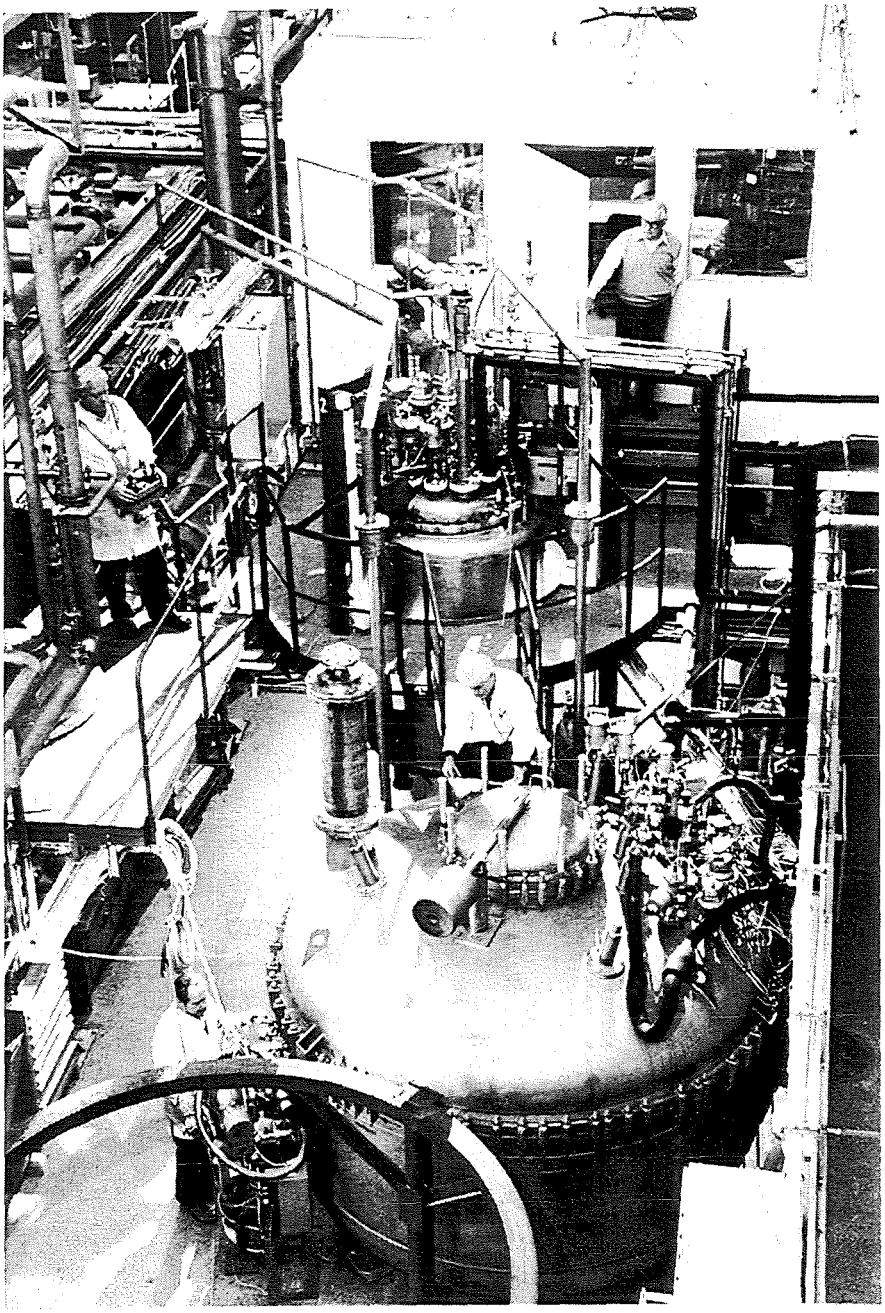

Fig.3: The HELITEX test facility

A schematic diagram of the test facility is shown in fig. 4. It consists of two cryostats with different functions. The first cryostat, which is connected to a helium refrigerator, is the so-called control cryostat accommodating a boiling LHe bath and whose refrigerating capacity is transferred via heat exchangers to the forced-circulated coolant flows. From the control cryostat helium, cooled down to 4.5 K in a first heat exchanger, is transferred via superinsulated transfer lines to the second cryostat, the so-called test cryostat. The latter cryostat which consists of the vacuum tank, the LN_2- and the 10 K helium-cooled shields accommodates the test section. The helium warmed up there and in the transfer lines is cooled down again in a second heat exchanger installed in the bath of the control cryostat. Helium forced-flow through the test section can be generated either by the He compressor of the refrigeration system (primary circuit using JT flow) or within a closed secondary circuit using cold helium pumps. Both helium pumps, a single-cylinder piston pump and a single-stage centrifugal pump, are operating while being immersed into the LHe bath of the control cryostat. The system pressure is controlled by the two control valves V1 and V2. Heating sections are located upstream of the test section to warm up the helium to a desired temperature. Four differential pressure flowmeters, i.e. orifices and venturi nozzles, are installed upstream of the heating section to determine the helium mass flow.

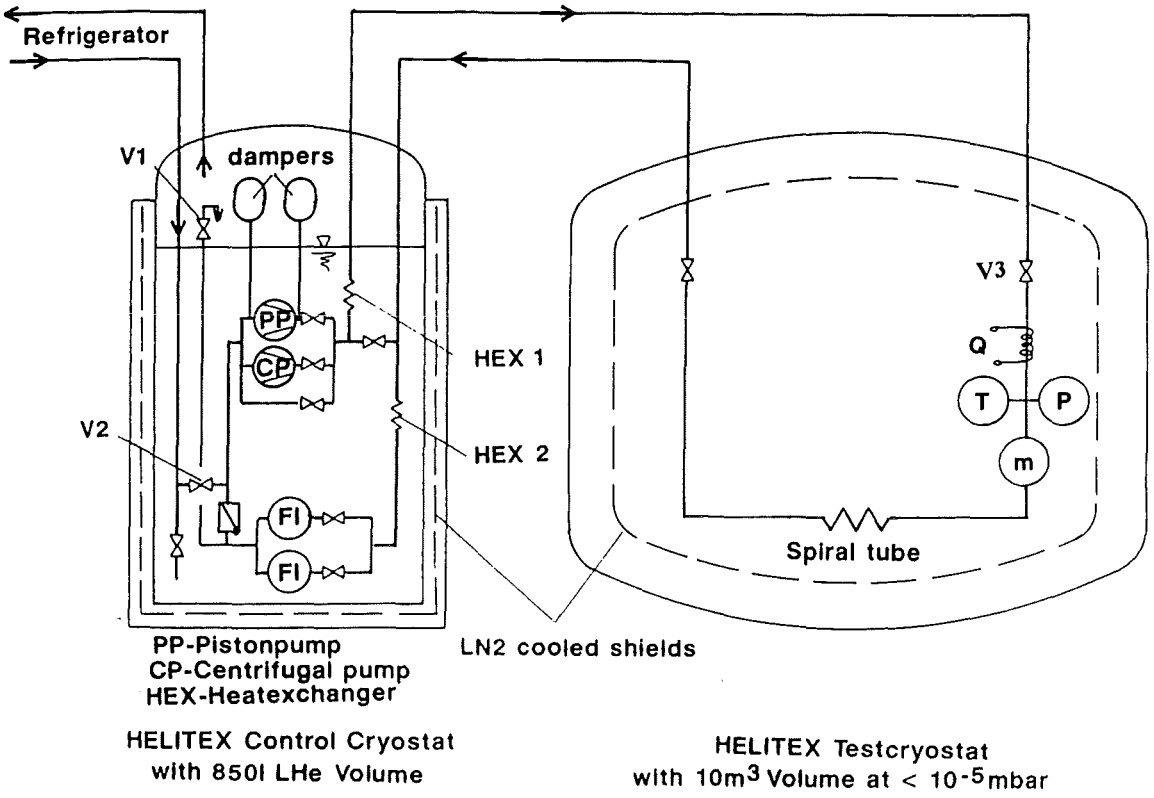

Fig.4: Schematic diagram of the HELITEX test facility

2.2 Test sections

Three test sections were used. With the first test section shown in fig. 5, transversal heat transfer between the jacket and the flow channel was measured. It consists of a piece of W7-X dummy conductor of 1.36 m length and a heating block made of copper, 200 mm in length which serves as the heater. The strands of the dummy conductor are made of copper wire of 0.55 mm inner diameter. The cross section of the heating block is large enough (30x40 mm) so that the temperature over the whole block is uniform which was comfirmed during the experiment. The heating block is pressed onto the conductor. Between both a piece of indium foil, 0.1 mm thick, is inserted to reduce the thermal resistance across the contact surface. By use of eight M6-bolts and cup-springs, an excellent thermal contact between the heating block and the conductor is guaranteed, also at low-temperatures. During the experiment, fluid temperature and pressure at the inlet and at the outlet of the conductor, mass flow through the conductor, temperature of the heating block and heating power supplied to the heating block were measured.

To investigate the thermal conductivity of the insulating layer, two different test sections were used. Each test section (fig. 6) consists of two W7-X conductors, each about 2 m in length. The main difference between these two test sections is the thickness of the insulating layer which is 1.2 mm in the one and 2.0 mm in the other test section. Helium at different temperatures could be circulated through the flow channels. The temperature difference resulted in transversal heat transfer from the 'hot' flow channel to the 'cold' flow channel. At the test section, helium temperature and pressure at the inlet, at the outlet and in the middle of each conductors and helium mass flow through both conductors were measured.

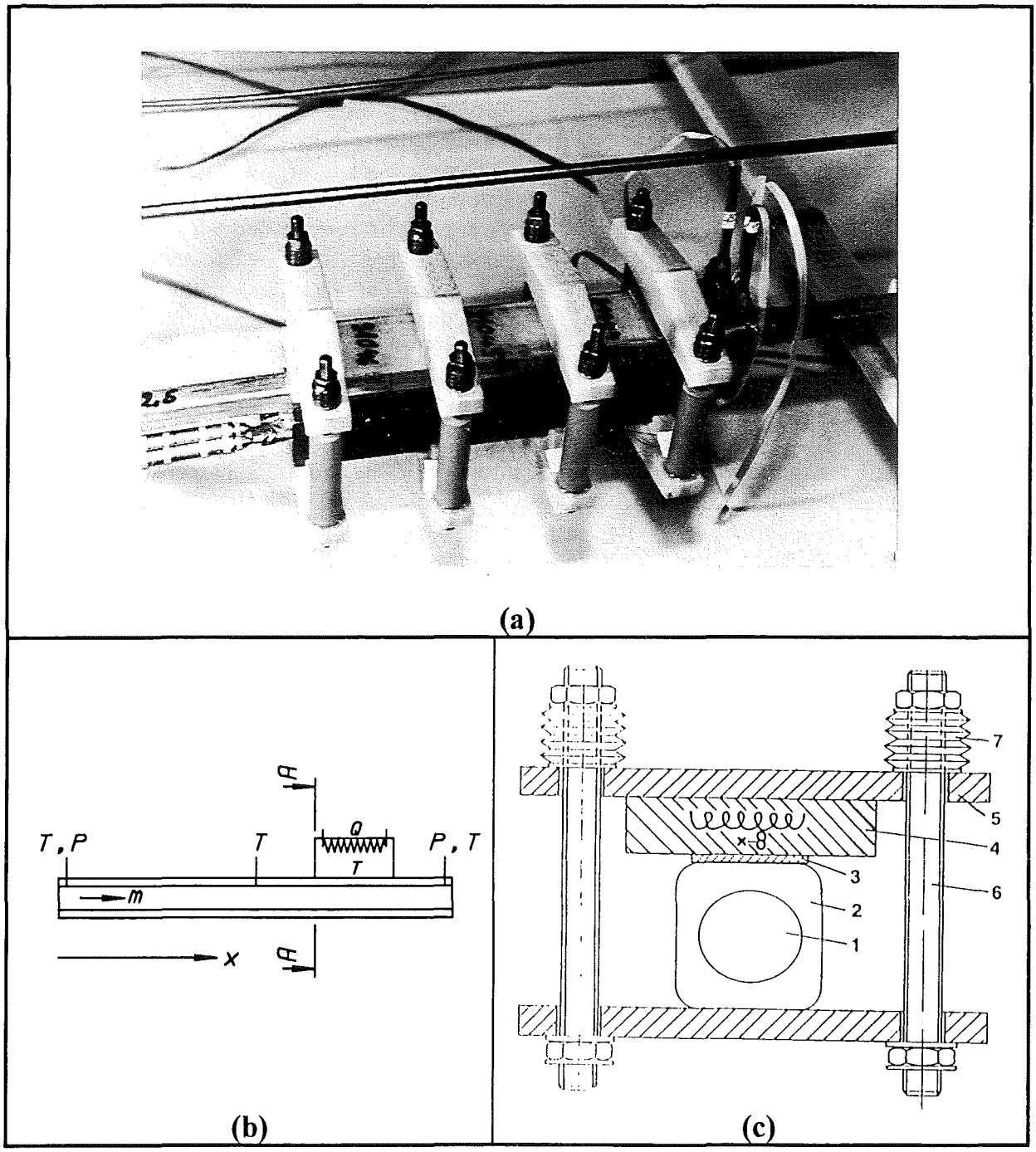

Fig. 5: The first test section

(a) Test section

(b) Test object with various measurements indicated

(c) Cross section of the test object:

1, flow channel; 2, jacket; 3. indium foil

4, heating block; 5, insulating layer,. 6, bolts;

7, conical disc; 8, T measurement

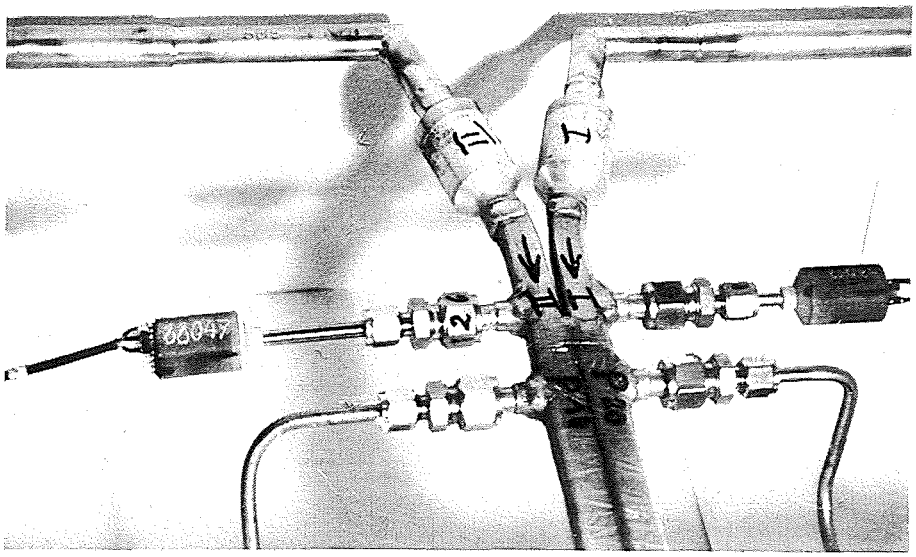

(a) *Inlet of the test section*

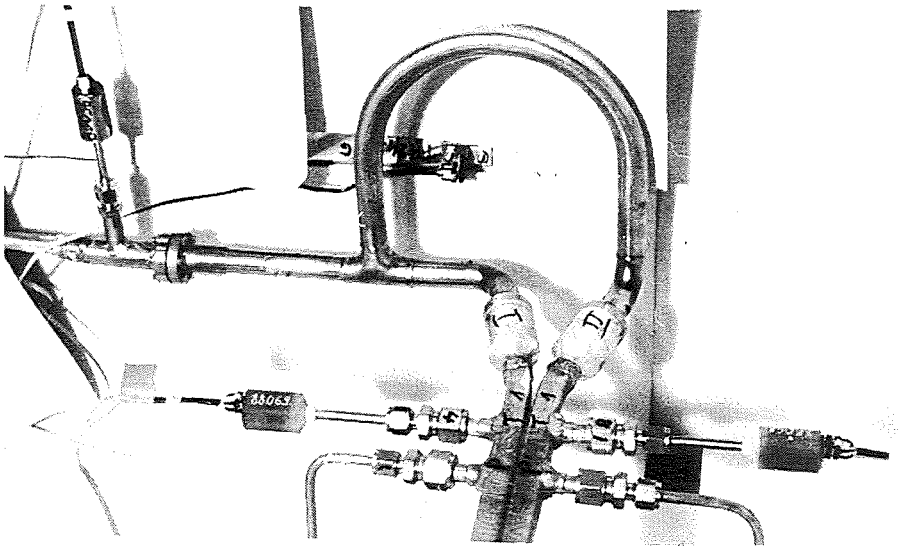

(b) *Outlet of the test section*

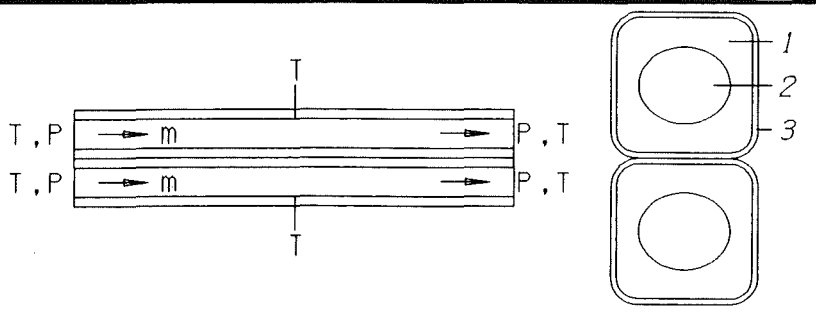

(c) *Schematic diagram of the test section*
1, jacket; 2, flow channel; 3, insulating layer
Measurements: T, temperature, P, pressure; m, mass flow

Fig. 6: Test section for the thermal conductivity of insulating layers

2.3 Test matrix

Table 1 summarizes thermohydraulic and geometric parameters of the conductors used in experiments. For comparison parameters of a proposed W7-X conductor are also shown in table 1.

Table 1: Thermohydraulic and geometric parameters			
Parameters	**Experiments**		**Proposed**
	1. test section dummy	**2./3. test section prototype**	
Strands			
Material	copper	copper/NbTi	copper/NbTi
Diameter (mm)	0.55	0.55	0.55
Number of strands	3x4x4x4	3x4x4x4	3x4x4x4
Cross section area (mm^2)	44.0x1.05	45.0x1.05	45.6x1.05
Jacket			
Material	AlMgSi1		
Dimension (mm^2)	14.8x14.8	14.8x14.8	14.8x14.8
Cross section area (mm^2)	140.1	138.4	135.5
Helium			
Pressure (MPa)	0.3 - 0.7	0.3 - 0.7	≈ 0.5
Temperature (K)	5.0 - 20.0	5.0 - 20.0	≈ 3.8
Mass flow (g/s)	0.3 - 2.5	0.3 - 2.5	≈ 0.6
Flow channel			
Shape	ellipse	ellipse	circle
Diameter (mm)	10.4/9.6	10.4/9.6	10.0
Cross section area (mm^2)	69.36	72.34	78.54
Helium area (mm^2)	23.16	25.14	30.66
Void fraction (%)	33.4	34.8	39.0
Wetted perimeter (mm)	308.0	308.0	308.0
Hydraulic diameter (mm)	0.300	0.340	0.442
Insulating layer			
Material	glass epoxy resin		
Thickness (mm)	---	1.2 and 2.0	1.2 and 2.0

The cross-section area of the jacket and of the strands was measured by determining their weight. The void fraction was found by filling water in the flow channel and determining the water weight.

2.4 Measurements

Temperature

Temperature was measured by carbon resistance thermometers (C100) which were calibrated in the range from 4 K to 30 K at the calibration laboratory of KfK/ITP. Figure 7 shows the maximal temperature deviation by repeated calibration procedures (three times). The reproducibility during the calibration is accurate to about 0.02 K. The coefficients of a polynomial function of nineth degree is optimized to correlate the relation between temperature and the electric resistance of the thermometer. Figure 8 shows the results. The symbols represent the calibration data, and the smooth curve is computed by the polynomial function. As can be seen, the polynomial function gives a smooth course and agrees well with the calibration data. Figure 9 presents the temperature deviation between the calibration results and the data calculated with the polynomial function. The polynomial function is accurate to better than 0.02K. the temperature error resulted by calibration and by polynomial functions is estimated to be less than 0.04 K.

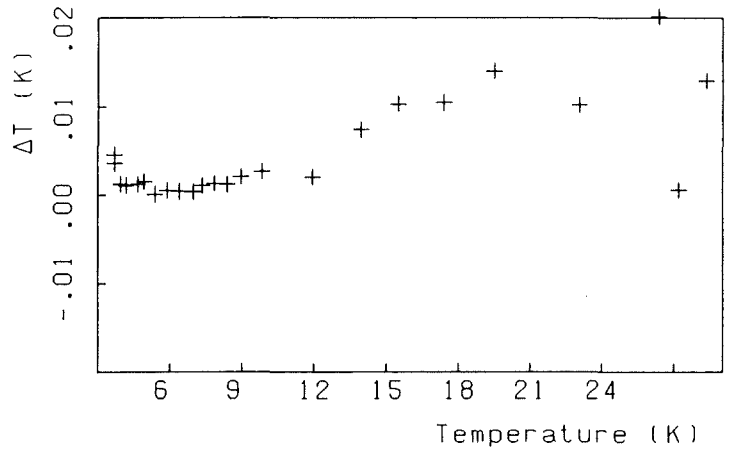

Fig. 7: Maximum temperature deviation by repeated calibration procedures

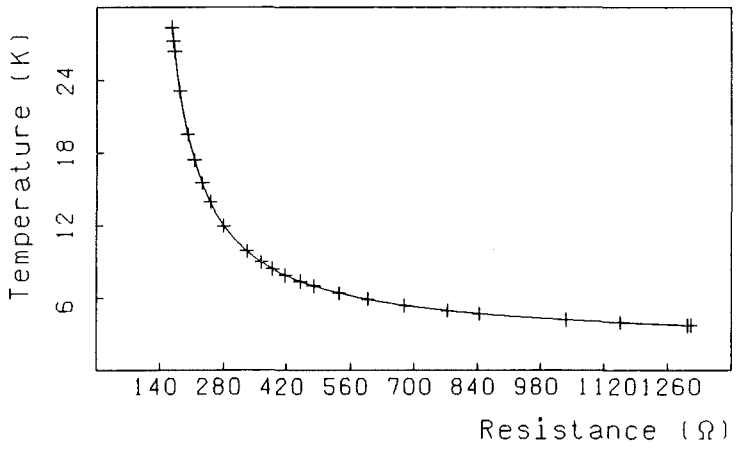

Fig. 8: Characteristics of thermometers
symbol (+) - calibration; line (—) - polymonial function

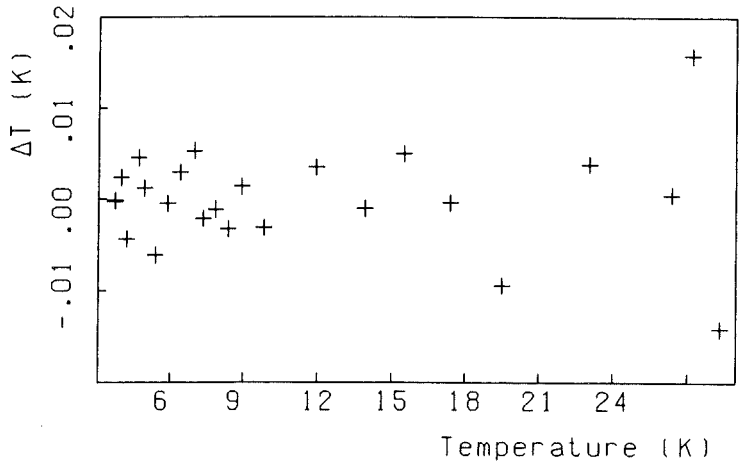

Fig. 9: Temperature deviation between the calibration results and the data calculated by polynomial funtion

Mass flow

Mass flow is measured by differential pressure flowmeters, i.e. by orifices and Venturi nozzles. Table 2 summarizes the dimensions of the flowmeters,

Table 2: Dimensions of the differential pressure flowmeters

Flowmeter	Type	D(mm)	d(mm)	β	L_1	L_2
FI4	orifice	5.0	1.20	0.24	1.0	1.0
FI5	venturi	4.0	1.20	0.30	--	--
FI6	orifice	5.0	1.90	0.38	1.0	1.0
FI7	orifice	5.0	1.90	0.38	1.0	1.0

where D is the pipe inside diameter, d is the proposed orifice diameter or the Venturi nozzle diameter, L_1 and L_2 are dimensional corrections for upstream and downstream tap locations, β is the so called beta ratio defined as d/D. The Stolz orifice equation

$$C = 0.5959 + 0.0312\beta^{2.1} - 0.184\beta^{8} + \frac{0.09L_1\beta^{4}}{(1-\beta^{4})} - 0.0337L_2\beta^{3} + \frac{91.71\beta^{2.5}}{Re_D^{0.75}} \qquad (1)$$

is accepted by the International Organization for Standardization [6] and by the german DIN [7] to calculate the discharge coefficient C of an orifice flowmeter. Re_D is Reynolds number referring to the pipe inside diameter,

$$Re_D = \frac{4 \cdot m}{\pi \cdot D \cdot \mu} \qquad (2)$$

where m is mass flow and μ dynamic viscosity. Fig. 10 shows the dependence of the discharge coefficient C on Reynolds number.

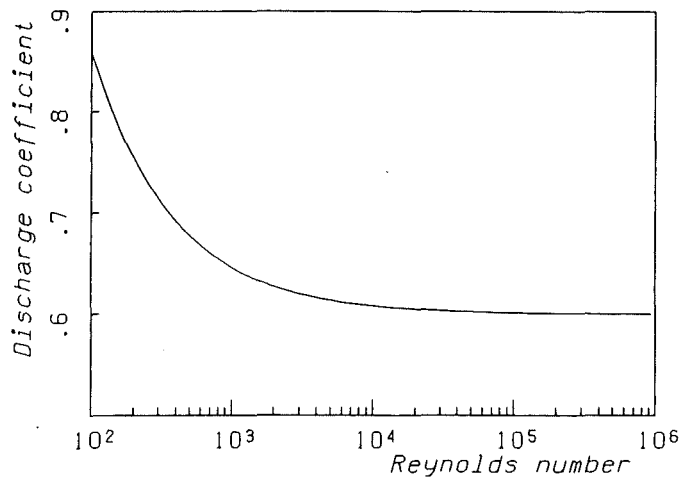

Fig.10: Discharge coefficient of orifices versus Reynolds number eq.(1), $\beta = 0.38$, $L_1 = 1.0$, $L_2 = 1.0$

The discharge coefficient decreases with increasing Reynolds number. In the range of high Reynolds number the last term of equation (1)

$$\frac{91.71\beta^{2.5}}{Re_D^{0.75}}$$

goes to zero and the discharge coefficient is then only dependent on geometric parameters. For Venturi nozzles the discharge coefficient is constant at high Reynolds number and equal to 0.98 [7]:

$$C = 0.98 \qquad (3)$$

Equation (1) and (3) are valid only for flowmeters with large diameters, e.g. $d \geq 12.5$ mm. The flowmeters used in the present work are outside the valid range of dimensions. Calibration of these flowmeters is therefore necessary. For simplicity the flowmeters were calibrated with water. For the Venturi nozzle it was found that at high Reynolds number (≥ 2000) the measured discharge coefficient agrees well with equation (3). For orifices the maximum Reynolds number achieved in the calibration is so high that the last term of eq.(1) is less than 1% of the discharge coefficient, i.e.

$$\frac{\dfrac{91.71\beta^{2.5}}{Re_{D,max}^{0.75}}}{0.5959 + 0.0312\beta^{2.1} - 0.184\beta^{8} + \dfrac{0.09L_1\beta^4}{(1-\beta^4)} - 0.0337L_2\beta^3} \leq 0.01$$

Figure 11 shows the calibration results for the mass flowmeters FI4 and FI6. The symbols represent the calibration data whereas the curves are the values computed by equation (1).

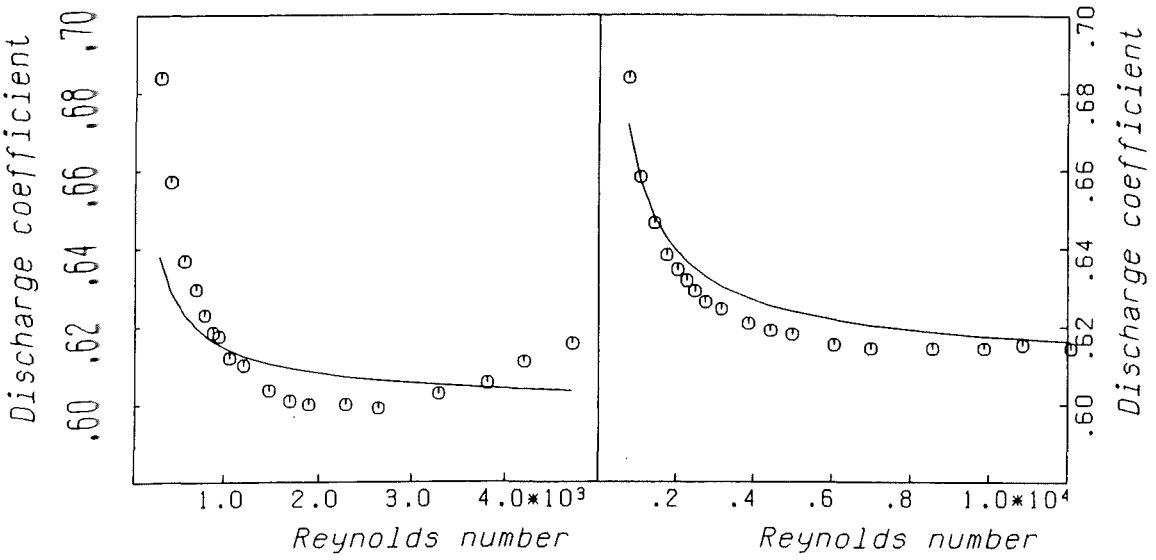

a) flowmeter FI4 b) flowmeter FI6

Fig.11: Calibrated discharge coefficient of flowmeters FL4 and FL6 using water

Deviation between the calibration results and the data calculated by equation (1) is large, especially for the orifice with small orifice diameter. Moreover, the calibration data show that the discharge coefficient does not always decreace asymtotically with increasing Reynolds number, but increaces slightly at high Reynolds number. It is doudtful to extrapolate the calibration results to higher Reynolds number ($\geq 10^4$) which is of interest for experiments. Therefore all the flowmeters were calibrated again in the Helitex test facility with supercritical helium by means of the calorimetric method under similar conditions as in the experiments. Mass flow was determined by heat balance:

$$m_h = \frac{Q}{h_2 - h_1} \tag{4}$$

where Q is the heating power, h_1 and h_2 are helium enthalpy at the inlet and at the outlet of the heating section. Figure 12 compares the mass flow measured by flowmeters m_f with that determined calorimetrically m_h. During the calibration procedure it was found that with the flowmeter FI 7 no stable flow of supercritical helium in the Helitex test loop was possible. Therefore, the flowmeter FI7 was excluded and not used in experiments. From the calibration data correction factors were determined for each flowmeter.

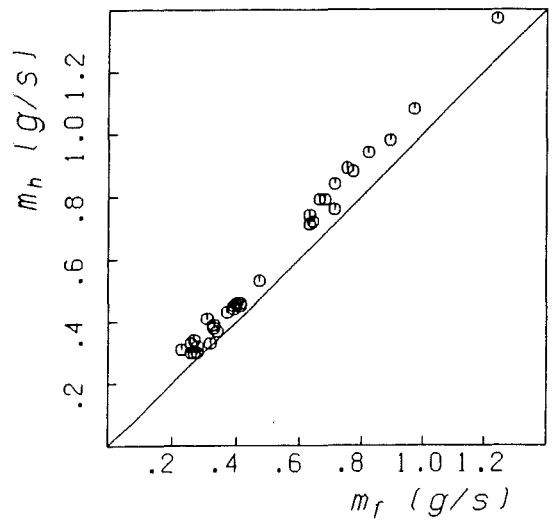

(a) flowmeter FI4 (orifice)

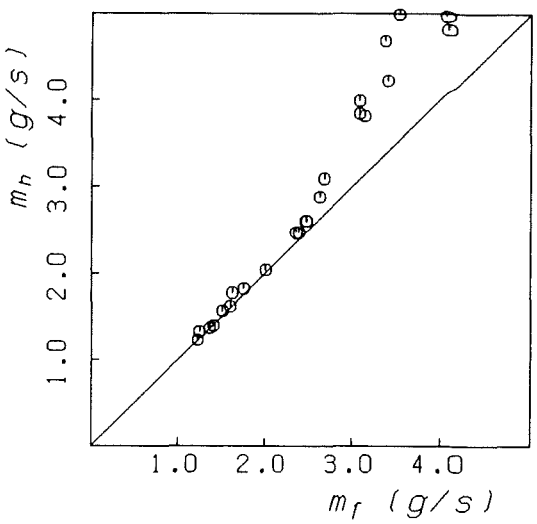

(b) flowmeter FI6 (orifice)

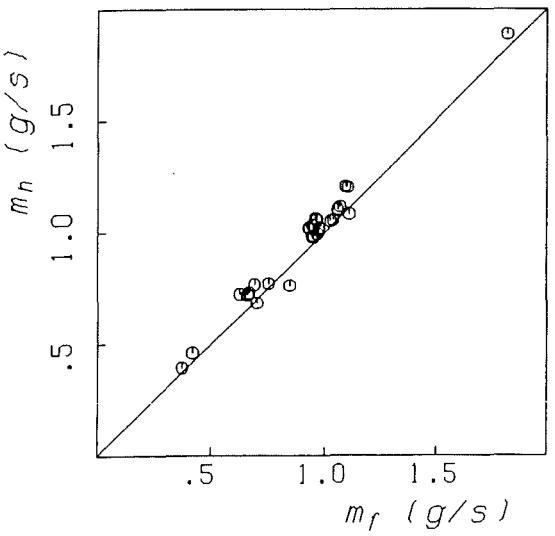

(c) flowmeter FI5 (Venturi)

Fig. 12: Comparison of mass flow measured by flowmeters with that determined calorimetrically

Pressure measurement

Pressure and pressure drop were measured by transducers which were located outside the apparatus at room temperature. The measurement error of pressure transducers should be less than 0.5% and that of differential pressure transducers is less than 0.2% of corresponding full scales.

3 Experimental results and discussion

The range of experimental parameters is shown in table 1. The thermophysical properties of helium needed to evaluate the experimental results are computed from [8]. The experimental data are summarized in appendix B, C, D and E.

3.1 Pressure drop

Figure 13 shows the measured relation between the friction factor and Reynolds number for the first test section (dummy conductor). The friction factor is defined as

$$f = \frac{d}{L}\frac{2 \cdot \Delta P}{\rho \cdot u^2}, \tag{5}$$

where d is the hydraulic diameter, L the length, ρ the density, ΔP the pressure drop and u the velocity.

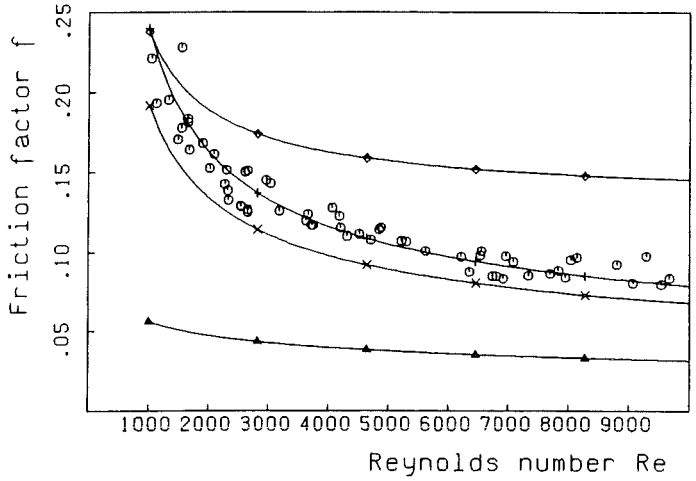

Fig.13: Friction factor versus Reynolds number:
⊗, measurement; Δ, Blasius; ◊, Katheder; x, Tada; +, equation (9)

For comparison, the Blasius equation, the equation of Katheder [9] and of Tada [10] are also presented in figure 13. The Blasius equation

$$f = \frac{0.3164}{\mathrm{Re}^{0.25}} \tag{6}$$

is valid for turbulent flow in smooth circular tubes. As can be seen, the friction factor in the W7-X conductor is roughly three times the values in an equivalent smooth circular tube. The Katheder's equation

$$f = \frac{1}{\alpha^{0.8}}\frac{23.0}{\mathrm{Re}^{0.78}} + 0.023 \tag{7}$$

overpredicts the test results. The Tada equation is a modified Prandtl-Karman equation

$$1/\sqrt{f} = 0.87 \ln\left(Re\sqrt{f}\right) - A \qquad (8)$$

The coefficient A was obtained by using the experimental data obtained from the DPC conductor and is equal to 3.0 [13]. The functional dependence of the friction factor on Reynolds number is described well by the Tada equation. However, the measured data are in average about 15% higher than the values calculated with the Tada equation. By using the present test results a optimum value for the coefficient A of equation (8) was found to be 3.3. The equation derived

$$1/\sqrt{f} = 0.87 \ln\left(Re\sqrt{f}\right) - 3.3 \qquad (9)$$

is also presented in figure 13. A good agreement is found between the experimental data and the calculated results.

Figure 14, 15, 16 and 17 show the measured friction factor in the four prototype-W7-X conductors used in the second and in the third test sections. For comparison, the test results of the dummy conductor and the equation (9) were also presented. As can be seen, the test results in the conductor No.1 of both test sections (fig.14 and fig.15) agree well with the data obtained in the dummy conductor and can be reproduced well by equation (9). Nevertheless, the test results of the conductor No.2 in both test sections deviate strongly from the data of the dummy conductor. At high Reynolds number the friction factor increases slightly with increasing Reynolds number. These unexpected results could be attributed to the measurement error of the mass flow through the second conductor.

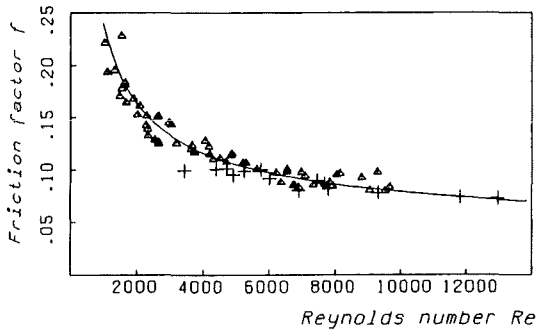

Fig.14: Friction factor for the first conductor of the second test section (+) compared to the results for dummy conductor (Δ) and equation (9) (—)
mass flow measured by the Venturi nozzle FI5

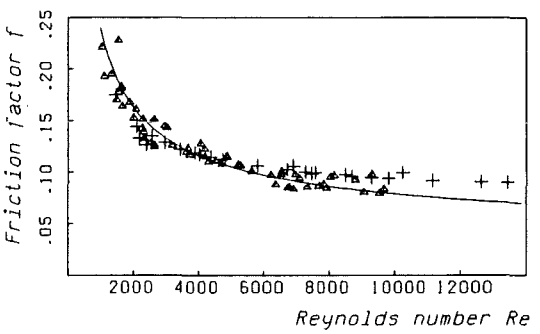

Fig.15: Friction factor for the first conductor of the third test section (+) compared to the results for dummy conductor (Δ) and equation (9) (—)
mass flow measured by the Venturi nozzle FI5

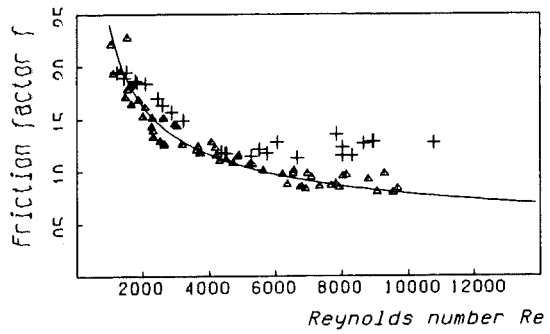

Fig. 16: Friction factor for the second conductor of the second test section
the results for dummy conductor (Δ) and equation (9) (—)
mass flow measured by the orifices FI4 and FI6

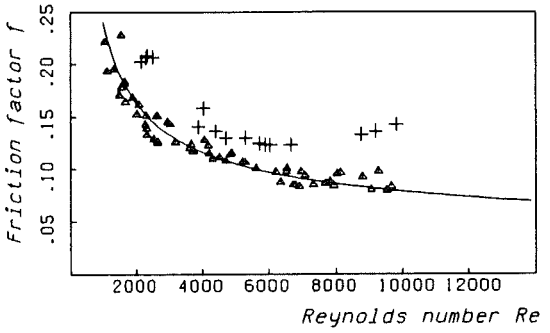

Fig. 17: Friction factor for the second conductor of the third test section
the results for dummy conductor (Δ) and equation (9) (—)
mass flow measured by the orifices FI4 and FI6

3.2 Heat transfer between flow channel and jacket

3.2.1 Theoretical method of evaluating the transversal heat transfer coefficient

3.2.1.1 General problem

For the test section shown in figure 5, it is not possible to distinguish experimentally the heat transfer between the jacket and helium from that between the jacket and the strands. Therefore, helium and the strands are considered as a unit, the so-called *flow channel*. On account of the large heat-transfer area between helium and the strands, the temperature difference between them is considered to be sufficiently small. The local heat transfer coefficient is then defined as

$$\alpha = \frac{q}{T_w - T_f}. \tag{10}$$

To determine the heat transfer coefficient experimentally, the local parameters, i.e. the fluid temperature T_f, the jacket temperature on the channel surface T_w and the heat flux q are required. As the structure of CICC is complicated and the possibilities of the measurement technology are limited, it is still not possible to measure these local parameters directly. Instead, a theoretical method was developed which does not serve to determine the local heat transfer coefficient, but to use a known equation of the heat transfer coefficient and to compare the calculated heat-transfer quantity with the measured one. The heat-transfer quantity is computed by

$$Q = \int_L dx \oint_S \alpha(\mathrm{Re}, \mathrm{Pr}, k, \cdots)\{T_w(s,x) - T_f(x)\}ds \tag{11}$$

where L is the heating length and S is the channel perimeter. If a known equation of the heat transfer coefficient is taken, $\alpha(\mathrm{Re}, \mathrm{Pr}, k, \cdots)$, the temperature distribution of helium as well as that in the jacket can be computed by solving the heat-conduction equation for the jacket and the conservation equations for helium simultaneously. The heat-transfer quantity Q is then computed according to equation (11). If the calculated heat quantity deviates from the measured one, the assumed equation of the heat transfer coefficient must be modified and the calculation procedure is repeated.

The major tasks involved in this calculation procedure consist in solving the conservation equations of helium and the heat-conduction equation for the jacket. The one-dimensional conservation equations of helium in the steady state are:

continuity

$$\rho \cdot u = const, \tag{12}$$

momentum conservation

$$\frac{dP}{dx} = -\frac{d(\rho \cdot u^2)}{dx} - \frac{f}{2d}\rho \cdot u^2, \tag{13}$$

and energy conservation

$$\frac{dh}{dx} = \frac{Q_l}{A \cdot u \cdot \rho} \tag{14}$$

which can be solved easily. By contrast, the three-dimensional heat-conduction equation cannot be solved analytically for the jacket. Also, a numerical solution is not practical because of high expenditure involved in terms of computing time and computer systems. However, this problem can be approximately solved by two-dimensional numerical analysis in cross sections perpendicular as well as parallel to the flow direction. For this purpose the computer code THECON (Two-dimensional HEat CONduction) was developed (see appendix A) for the non-linear steady-state two-dimensional analysis of the temperature distribution.

3.2.1.2 Heat conduction perpendicular to the flow direction

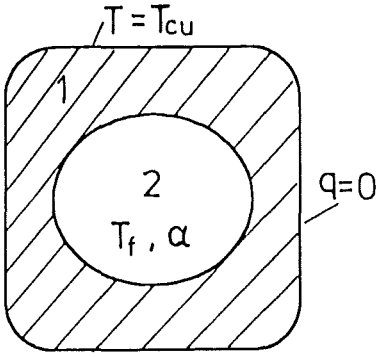

Fig.18: Cross-section perpendicular to flow direction. 1, jacket; 2, flow channel

The basic equations for the two-dimensional heat conduction in the cross-section shown in figure 18 are:

Fourier heat-conduction equation

$$\frac{\partial}{\partial X}\left(\lambda\frac{\partial\theta}{\partial X}\right)+\frac{\partial}{\partial Y}\left(\lambda\frac{\partial\theta}{\partial Y}\right)=0, \tag{15}$$

convective boundary condition at the surface of the flow channel

$$\left[\frac{1}{\theta}\frac{\partial\theta}{\partial n}\right]_w=\frac{\alpha}{\lambda}, \tag{16}$$

Dirichlet boundary condition at the surface in contact with the heating block

$$\theta_{cu}=\left[T-T_f\right]_{cu}=const, \tag{17}$$

and the Neumann boundary condition for the remaining insulated surfaces

$$\frac{\partial\theta}{\partial n}=0 \tag{18}$$

where θ is the difference between the jacket temperature and the fluid temperature. The heat quantity transferred from the jacket to the flow channel is computed by

$$Q_l=\oint_S\lambda\frac{\partial\theta}{\partial n}ds \tag{19}$$

The temperature of the heating block T_{cu} is measured and the helium temperature T_f can be computed referring to the measured inlet condition and solving the fluid conservation-equations. If the heat transfer coefficient α is given, the temperature distribution in the jacket

can be calculated. Figure 19 shows the temperature distribution in the jacket in case of T_{cu}=10 K, T_f=5 K and $\alpha = 2000 W / m^2 K$.

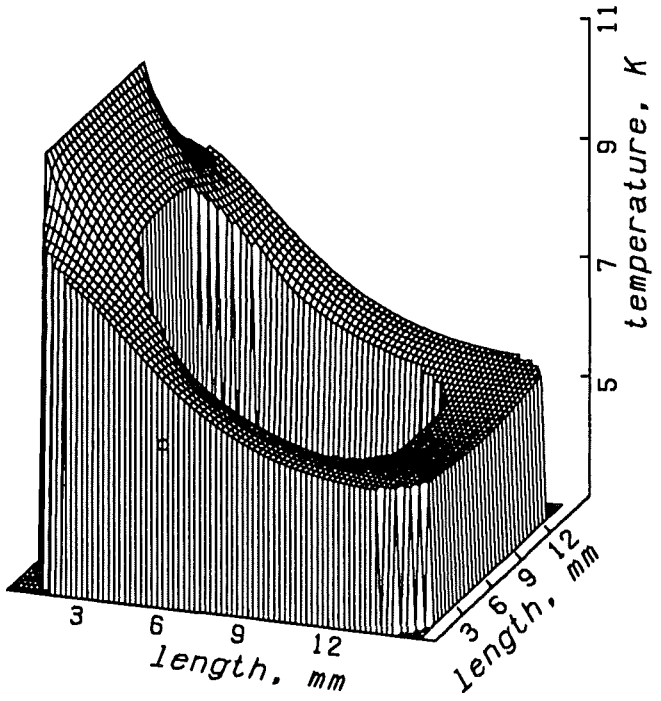

Fig.19: Temperature distribution in jacket

As expected, the temperature at the channel surface differs strongly along the wetted perimeter. On the side facing the heating block, the temperature is a little lower than that of the heating block, whereas on the opposite side it is nearly the same as the fluid temperature. From the temperature distribution, the heat flux distribution is determined and, finally, the heat-transfer quantity by integrating the heat flux over the channel surface. Figure 20 shows the heat flux distribution at the surface of the flow channel.

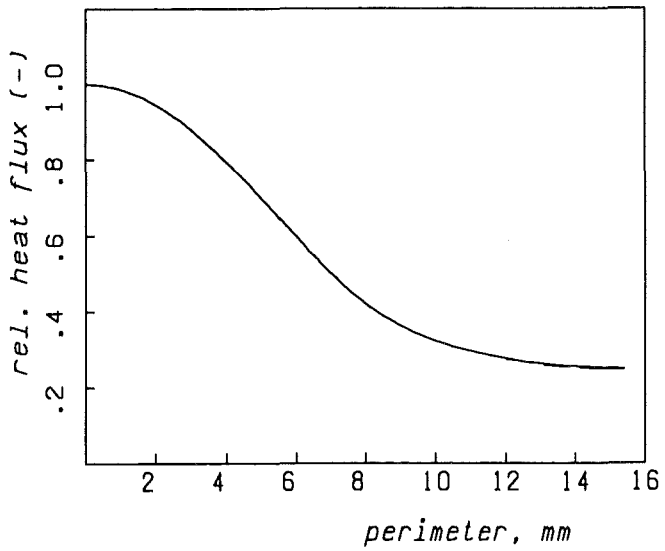

Fig.20: Heat flux distribution at flow channel surface

According to equations (15) to (19), the heat-transfer quantity can be expressed as a function ofother parameters

$$Q_l = f(T_{cu}, T_f, \lambda, \alpha) \tag{20}$$

If the value of the thermal conductivity of the jacket is taken to be constant, equation (20) is rewritten

$$Q_l = f_Q\left((T_{cu} - T_f), \lambda, \frac{\alpha}{\lambda}\right) = f_Q\left(1, \lambda_0, \frac{\alpha}{\lambda}\right) \cdot (T_{cu} - T_f) \cdot \frac{\lambda}{\lambda_0} \tag{21}$$

i.e.

$$Q_l \cdot \frac{\lambda_0}{\lambda} \cdot \frac{1}{T_{cu} - T_f} = Q_0 = f_Q\left(1, \lambda_0, \frac{\alpha}{\lambda}\right) \tag{22}$$

Equation (22) indicates that the heat-transfer quantity Q_l is proportional to the temperature difference $T_{cu} - T_f$ and to the thermal conductivity λ of the jacket. The quantity Q_0 defined in equation (22) depends only on the ratio α / λ. Figure 21 shows the dependence of Q_0 on the ratio α / λ for the W7-X conductor and for $\lambda_0 = 40 W / mK$.

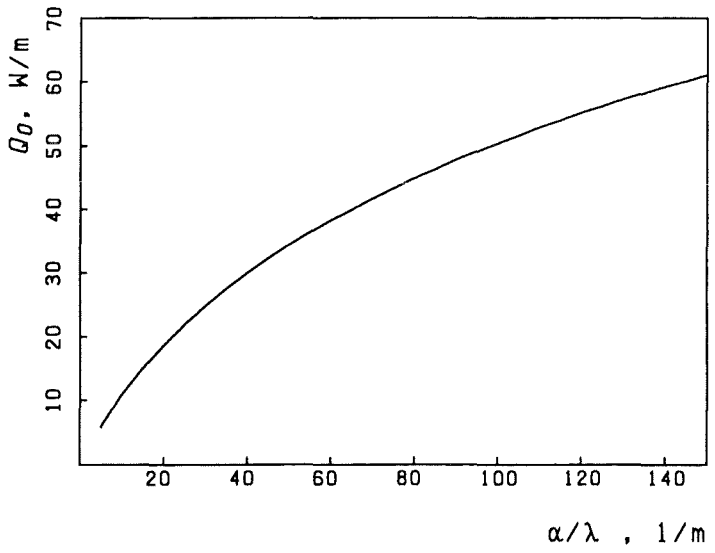

Figure 21: heat quantity Q_0 versus the ratio α / λ

3.2.1.3 Heat conduction parallel to the flow direction

For the study of the heat conduction in the cross-section parallel to the flow direction, the original three-dimensional cable-in-conduit conductor is simplified to an equivalent two-dimensional conductor with a rectangular flow channel, as shown in figure 22.

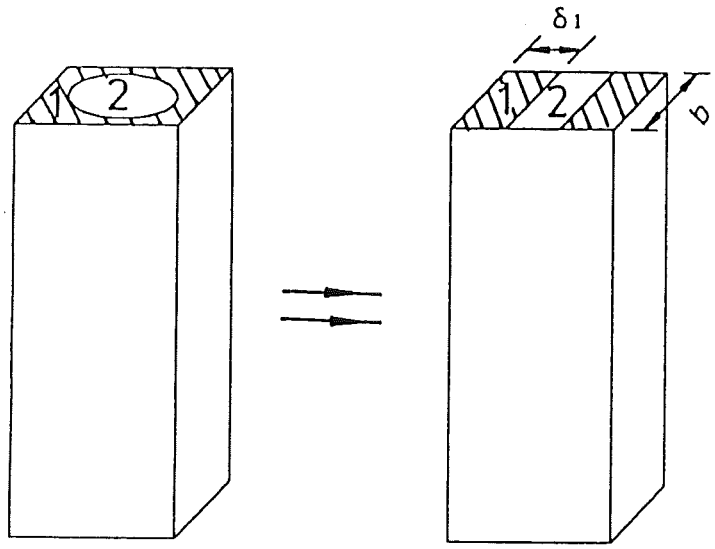

Figure 22: equivalent conductor for heat conduction parallel to the flow direction. 1, jacket; 2, flow channel

The heat transfer between the jacket and the flow channel takes place only at the channel surface near the heating block. The thickness δ_1 and the width b of the equivalent jacket wall are obtained by application of the following two conditions: 1, the heat quantity transferred into the equivalent rectangular flow channel is equal to that transferred into the original one; and 2, the average length of the heat-flow path in the jacket is geometrically coupled with the average width of the heat-transfer surface.

Solving the two-dimensional heat-conduction equation for the equivalent jacket numerically, we obtain the temperature distribution and the heat-flux distribution at the surface of the flow channel, which is shown in figure 23. As can be seen, due to the axial heat conduction the heat quantity transferred from the jacket to the flow channel is partly beyond the heating length. The ratio of the heat quantity transferred beyond the heating length to the entire heat-transfer quantity depends on the ratio α / λ, as shown in figure 24.

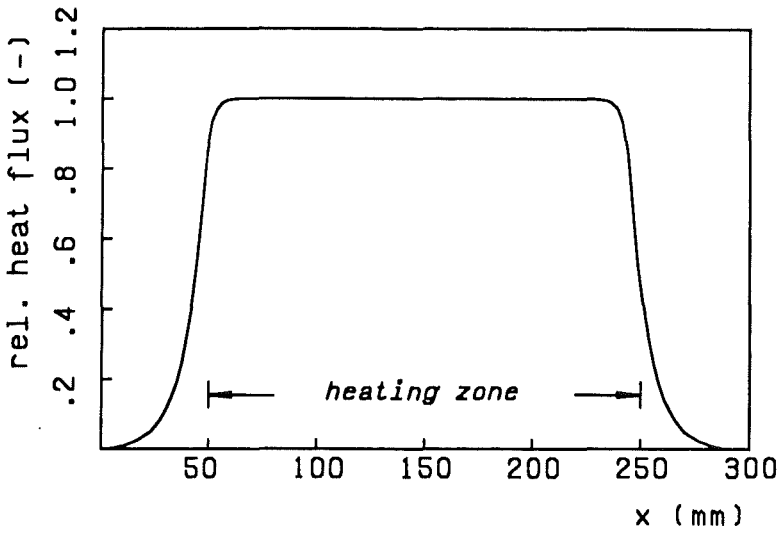

Figure 23: heat flux distribution in the flow direction

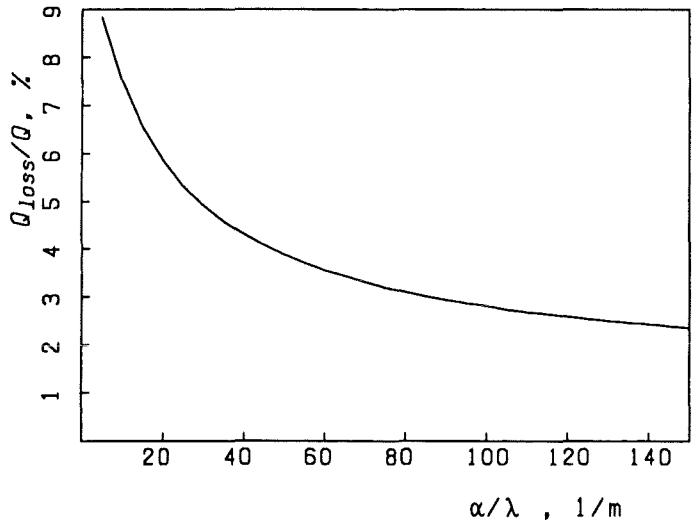

Figure 24: heat quantity transferred outside the heating zone versus the ratio α / λ

3.2.1.4 Calculation procedure

The procedures under the theoretical method will be explained below. First of all, a known functional relation between the heat transfer coefficient and other parameters is established,

$$\alpha = c \cdot \alpha(\mathrm{Re}, \mathrm{Pr}, k, \cdots) \tag{23}$$

where c is a correction factor. Now, the purpose of the calculation procedure is to determine the correction factor so that the calculated heat quantity agrees with the measured one. The entire heating length of the flow channel is divided into N sub-zones, as shown in figure 25.

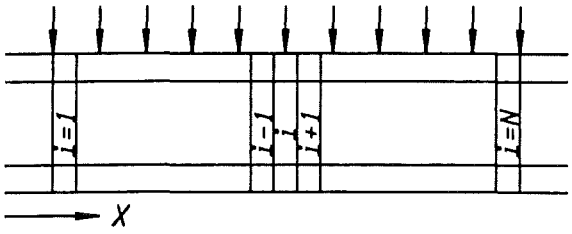

Figure 25: division of the heating length for 2D analysis

For a considered sub-zone i, the heat transfer coefficient is calculated by taking the flow parameters in the preceding sub-zone i-1. With the help of the numerical analysis of the two-dimensional heat conduction perpendicular to the flow direction, the heat quantity transferred in the sub-zone i is determined (see figure 21). Then the fluid temperature and pressure in the sub-zone i are computed by means of the helium conservation equations. As the flow parameters at the inlet are measured, the calculation procedure can be performed step by step from the inlet to the outlet over the entire heating length. The heat-transfer quantity within the heating length is then computed by adding up the heat-transfer quantities in all sub-zones

$$Q_h = \sum_{i=1}^{N} Q_{l,i} \Delta x_i \tag{24}$$

The heat transfer coefficient and the thermal conductivity of the jacket, averaged over the entire heating length, are determined by

$$\bar{\alpha} = \frac{1}{L} \sum_{i=1}^{N} c \cdot \alpha(\mathrm{Re}_i, \mathrm{Pr}_i, k_i, \cdots) \Delta x_i \tag{25}$$

$$\bar{\lambda} = \frac{1}{L} \sum_{i=1}^{N} \lambda_i \cdot \Delta x_i \tag{26}$$

With the ratio $\bar{\alpha} / \bar{\lambda}$, the quantity of heat transferred outside the heating zone Q_{loss} can be calculated (see figure 24). The total heat-transfer quantity is

$$Q_c = Q_h + Q_{loss} \tag{27}$$

If there is a large deviation between the calculated heat-transfer quantity and the measured one, $Q_c - Q_m$, a new correction factor has to be determined by solving the following equation

$$\frac{Q_m}{Q_c} = \frac{f_Q\left(1, \lambda_0, \frac{c \cdot \bar{\alpha}}{\bar{\lambda}}\right)}{f_Q\left(1, \lambda_0, \frac{\bar{\alpha}}{\bar{\lambda}}\right)} \tag{28}$$

Function f_Q is defined by equation (22) and shown in figure 21. Using the new correction factor, the same calculation procedure is repeated until the deviation $Q_c - Q_m$ is sufficiently small. Figure 26 shows the flow diagram of the calculation procedure.

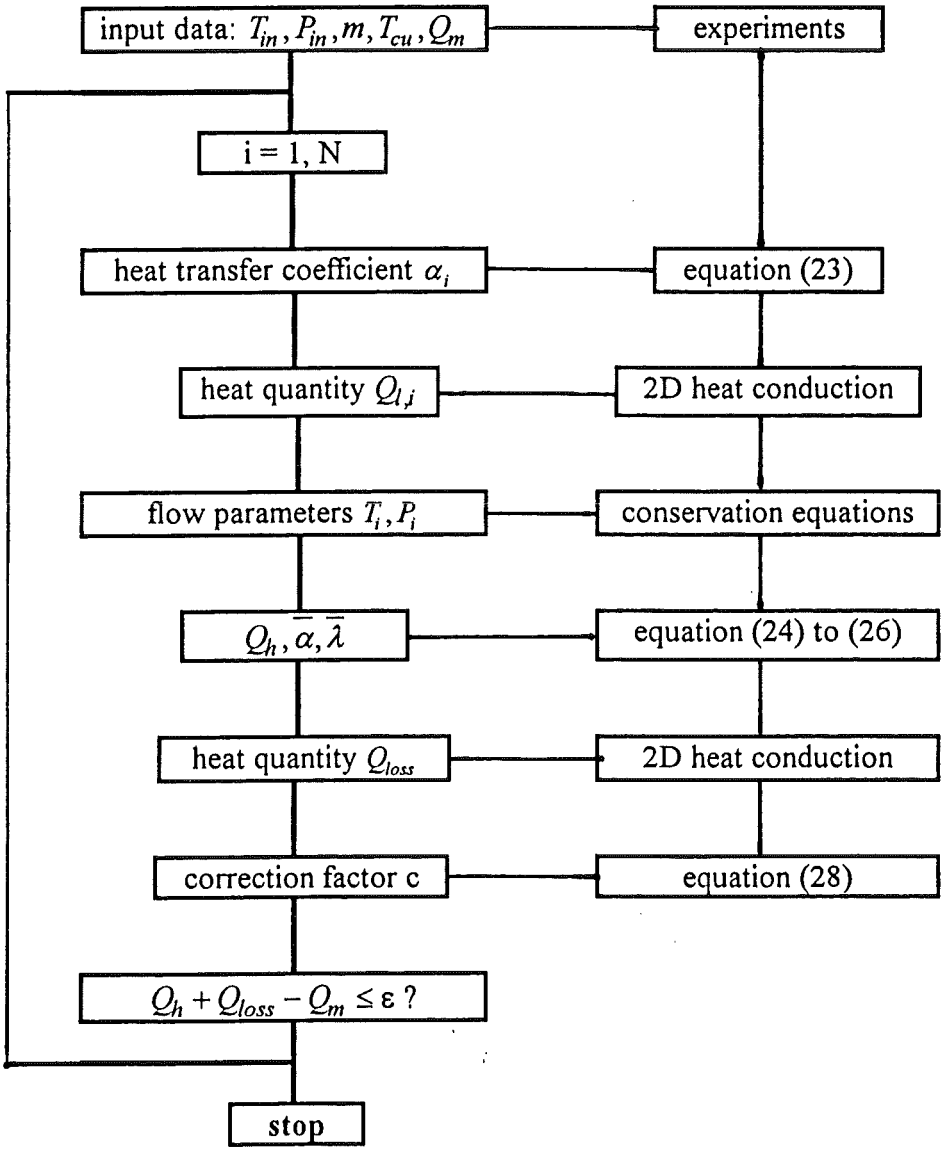

Figure 26: Flow diagram to determine the heat transfer coefficient

The finally determined correction factor represents the ratio of the measured heat transfer coefficient to that calculated with the equation $\alpha(\mathrm{Re}, \mathrm{Pr}, \mathrm{k}, \cdots)$. For all the M measurement data, the average value and the standard deviation of the correction factor are computed by

$$\mu = \frac{1}{M}\sum_{j=1}^{M} c_j \tag{29}$$

$$\sigma = \sqrt{\frac{1}{\mathrm{M}-1}\sum_{\mathrm{j}=1}^{\mathrm{M}}\left(\frac{\mathrm{c_j}-\mu}{\mu}\right)^2} \tag{30}$$

Substituting the correction factor c in equation (23) by its average value μ, we obtain an equation of the heat transfer coefficient

$$\alpha = \mu \cdot \alpha(\mathrm{Re}, \mathrm{Pr}, \mathrm{k}, \cdots) \tag{31}$$

which, on the average, reproduces the measured results accurately and whose quality is represented by the standard deviation of the correction factor.

3.2.2 Experimental results

Figure27 shows the experimental results.

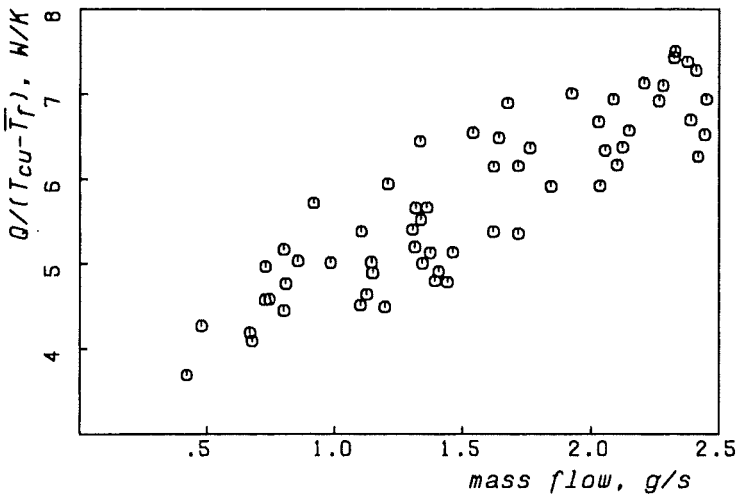

Figure 27: Experimental results for transversal heat transfer from the dummy conductor

Here $\overline{T}_f$ is the fluid temperature averaged over the inlet and the outlet temperature

$$\overline{T}_f = \frac{T_{f,in} + T_{f,ex}}{2} \tag{32}$$

The parameter, $Q/(T_{cu} - \overline{T}_f)$, represents the effective thermal conductance, which increases with increasing mass flow. The heat transfer between the jacket and the flow channel is obviously dependent on the flow conditions and cannot be described by pure heat conduction.

Figure 28 compares the test results with the Dittus-Boelter equation

$$\mathrm{Nu} = \frac{\alpha \cdot d}{k} = \cdot 0.023 \cdot \mathrm{Re}^{0.8}\,\mathrm{Pr}^{0.4} \quad . \tag{33}$$

At low Reynolds number the measured Nusselt number is much higher than the calculated data, whereas at high Reynolds number the Dittus-Boelter equation overpredicts the measured results. This systematic deviation indicates that the heat transfer between the jacket and the flow channel cannot be described accurately by pure convective heat transfer.

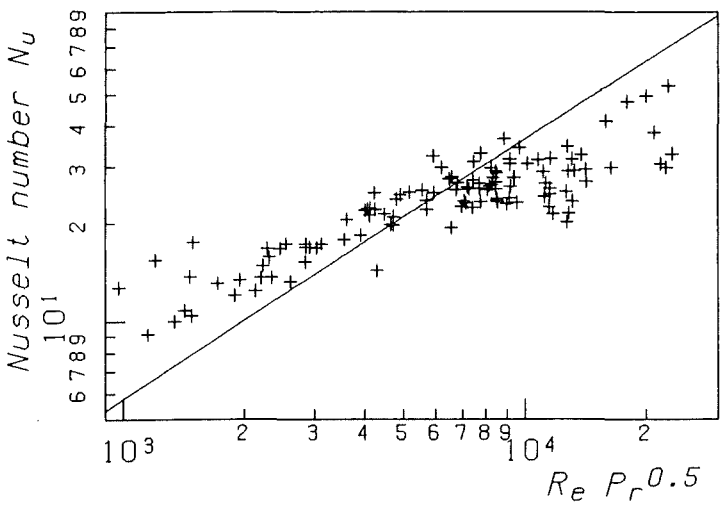

Fig. 28: Experimental heat transfer data (+) compared with the Dittus-Boelter equation (—)

3.2.3 A new model for transversal heat transfer in CICC's

As mensioned above that the transversal heat transfer between the flow channel and the jacket can not be described accurately by pure heat conduction or by pure heat convection. Therefore, a new model has to be developed in order to be able to describe the transversal heat transfer in CICCs.

For this purpose, the heat-transfer surface between the jacket and the flow channel is simplified to a straight one, as shown in figure 29.

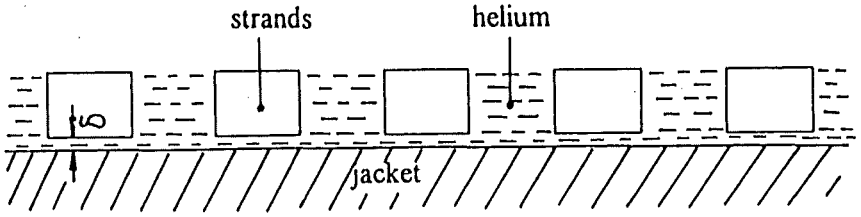

Figure 29: heat transfer mechanisms in CICC

The strands are assumed to be rectangular. In the one part of the surface A_2, strands are located close to the jacket. There is a thin film of helium between both. On the remaining surface A_1, strands are far away from the jacket and the jacket surface is flooded with helium. Heat transfer takes place by two different mechanisms: on the surface A_1, heat is transferred from the jacket to helium by heat convection. The heat-transfer quantity is computed by

$$Q_1 = A_1 \cdot \alpha_1 (T_w - T_f) \tag{34}$$

where α_1 is the convective heat transfer coefficient. On the surface A_2, heat transfer takes place via heat conduction through the thin helium film to the strands. The corresponding heat-transfer quantity is calculated by

$$Q_2 = A_2 \cdot \frac{k}{\delta} \cdot (T_w - T_f) \tag{35}$$

where δ is the average thickness of the helium film. The entire heat-transfer quantity is composed from both parts

$$Q = Q_1 + Q_2 = \left(A_1 \alpha_1 + A_2 \frac{k}{\delta} \right) (T_w - T_f) = A \cdot \alpha \cdot (T_w - T_f) \tag{36}$$

where A is the total heat-transfer surface and α is the effective heat transfer coefficient defined by

$$\alpha = \frac{A_2}{A} \frac{k}{\delta} + \frac{A_1}{A} \alpha_1 \tag{37}$$

The effective Nusselt number is calculated by

$$Nu = \frac{\alpha \cdot d}{k} = (1 - f_A)\frac{d}{\delta} + f_A \cdot \frac{\alpha_1 \cdot d}{k} = f_A (Nu_0 + Nu_1) \tag{38}$$

with

$$Nu_0 = \frac{1 - f_A}{f_A} \cdot Nu_2 \tag{39}$$

$$Nu_2 = \frac{d}{\delta} \tag{40}$$

$$f_A = \frac{A_1}{A_1 + A_2} = \frac{A_1}{A} \tag{41}$$

The Nusselt number Nu_2, finally Nu_0, represents the heat conduction through the helium film and depends only on the geometry of the flow channel. The Nusselt number Nu_1 stands for the convective heat transfer between the jacket and helium. By taking a known value for Nu_0 and a known function for Nu_1, the area ratio f_A is considered as a correction factor and can be determined by the method described in figure 26. If the Dittus-Boelter equation is used to calculate convective heat transfer, it is found that a constant Nusselt number of Nu_0=17.5 leads to a minimum standard deviation of the area ratio (17.0%). The corresponding average value of the area ratio is equal to 0.53. This indicates that 53% of the flow-channel surface is flooded with helium. These new equations have been developed:

$$Nu = f_A \cdot Nu_1 + (1 - f_A) Nu_2 \tag{42}$$

$$Nu_1 = 0.023 \cdot Re^{0.8} Pr^{0.4} \tag{43}$$

$$Nu_2 = \frac{d}{\delta} = 19.7 \tag{44}$$

$$f_A = 0.53 \tag{45}$$

The constant Nusselt number Nu_2=19.7 makes evident that the average thickness of the helium film between the jacket and the strands is about 5% of the hydraulic diameter, i.e. the helium film is about 15 μm. Fig. 30 compares the data calculated by eq.(42) - eq.(45) with the experimental results. A good agreement is obtained.

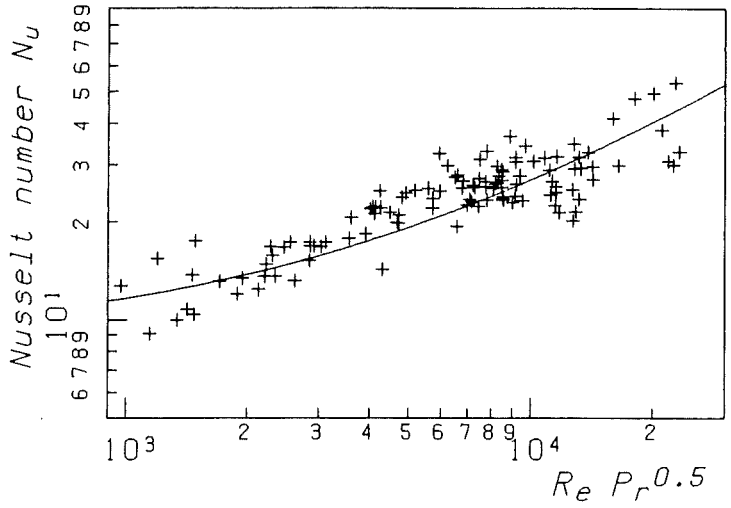

Fig.30: Experimental heat transfer data (+) compared with equation 42 (—)

It should be emphasized that the developed new model, equations (38) to (41), can be also applied to other cable-in-conduit conductors. Nevertheless, the optimized equations (42) to (45) are only valid for the W7-X conductor used and for the particular operating conditions tested. For other conductors with different cabling structures and for other operating conditions, the area ratio f_A and the average thickness δ could deviate from the values determined in the present work.

3.3 Heat conduction through the insulating layer

To evaluate the thermal conductivity of the insulating layer, a self-developed method was used which is similar to the method for evaluating the transversal heat transfer coefficient described in chapter 3.2.1. This method contains the following steps:

- Take a constant value for the thermal conductivity
- Calculate the distribution of the fluid temperature in both flow channels by solving the conservation equations of helium, eq.(12) to eq.(14), and the heat conduction equation, eq.(15), for solid materials (jacket and insulating layer) by using the THECON computer code.
- Modify the assumed value of the thermal conductivity, unless the calculated temperature distribution of helium agrees with the measured results.

For numerical simulation with the THECON code the original three-dimensional conductor is simplified to a two-dimensional conductor, as shown in Fig.31.

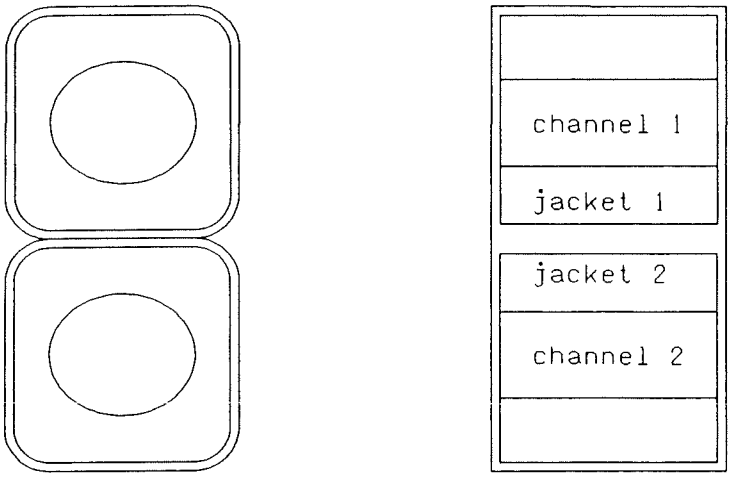

Original conductor Simplified conductor

Fig.31: Original and simplified conductors for numerical analysis with the THECON code

The width of the equivalent cross section is set equal to the original width of 14.8 mm. The thickness of the jacket wall δj was determined according to the requirement that the thermal resistance of the jacket is identical in both the original and the simplified conductors. The thermal resistance of the original conductor can be computed by

$$\frac{Q}{\Delta T} = f_Q\left(\lambda_0, \frac{\alpha}{\lambda}\right) \cdot \frac{\lambda}{\lambda_0} \tag{46}$$

Function f_Q is defined in eq.(22) and presented in figure 21. The thermal resistance of the simplified conductor is calculated by

$$\frac{Q}{\Delta T} = \frac{\alpha \cdot \lambda}{\lambda + \alpha \cdot \delta j} \tag{47}$$

Combining equation (46) and (47) the jacket wall thickness of the simplified conductor is solved

$$\delta_j = \frac{\lambda_0}{f_0(\lambda_0 + \alpha/\lambda)} - \frac{\lambda}{\alpha} \tag{48}$$

The thickness of the insulating layer of the simplified conductor is determined by averaging the thickness of the original insulating layer over the entire width, i.e.

$$\delta_i = \frac{1}{\frac{1}{b}\int_0^b \frac{1}{\delta_i(x)}\,dx} \tag{49}$$

At the boundary surfaces of both flow channels convective boundary conditions are used and equation (42) to (45) are taken to compute the heat transfer coefficient.

Figure 32 shows an example of the calculated temperature distribution of helium in both flow channels compared to the measured data. For the experimental condition considered the calculated temperature distributions agree well with the measured results, if an effective thermal conductivity λ_i of 0.08 W/mK for the insulating layer is taken.

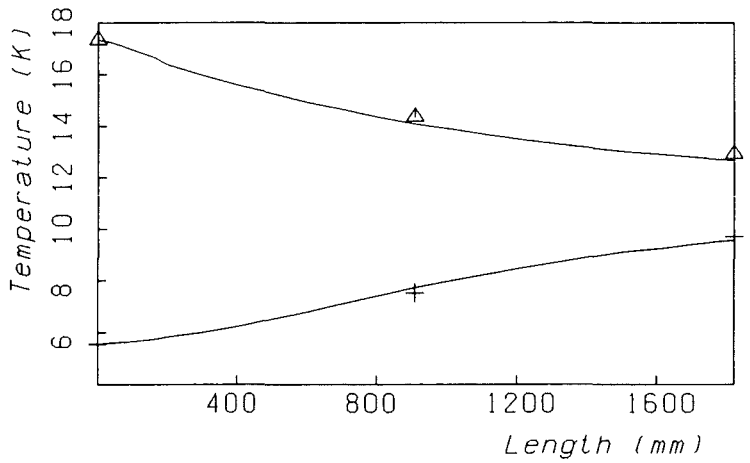

Fig.32: Calculated temperature distribution of helium (—, λ_i=0.08 W/mK) in comparison with measured data (Δ, hot channel; +, cold channel)
$m_1 = 0.39$ g/s, $m_2 = 0.27$ g/s, $P_1 = P_2 = 3.0$ bar

Fig.33 shows the calculated heat flux at the channel surface and the transferred heat power as function of the length in the flow direction. The heat flux decreaces in flow direction due to the decreasing temperature difference. Over the entire length (1.8 m) a heat power of about 10W is transfered from the hot to the cold flow channel.

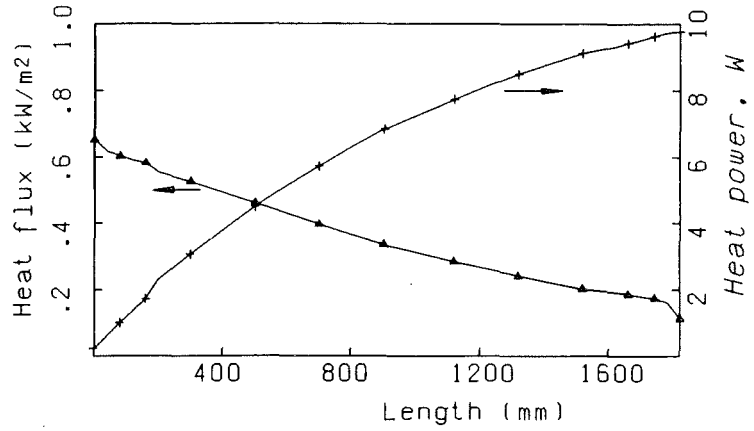

Fig.33: Calculated heat flux distribution (Δ) and transferred heat power (+)
$m_1 = 0.39$ g/s, $m_2 = 0.27$ g/s, $P_1 = P_2 = 3.0$ bar

Figure 34 shows the calculated transversal temperature distribution in both conductors. The temperature drop across the insulating layer is about 90% of the entire temperature difference between two flow channels. The thermal resistance of the jacket is negligible. The thermal resistance between flow channel and jacket increases with decreasing mass flow. At low mass flow which corresponds to the designed operating conditions, it reaches about 10% of the entire transversal thermal resistance.

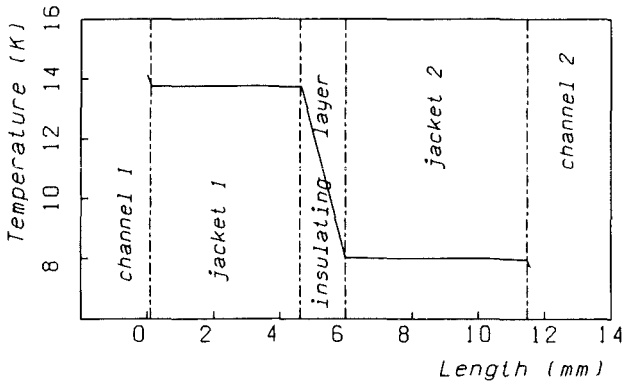

Fig.34: Calculated transversal temperature distribution in both conductors
$m_1 = 0.39$ g/s, $m_2 = 0.27$ g/s, $P_1 = P_2 = 3.0$ bar

Numerical simulations were performed for every measurement to evaluate the effective thermal conductivity of the insulating layer. Figure 35 presents the thermal conductivity versus the average temperature of the insulating layer. The test results obtained in both test sections agree well with each other. The thermal conductivity increases with increasing temperature and agrees satisfyingly with the data available in the literature.

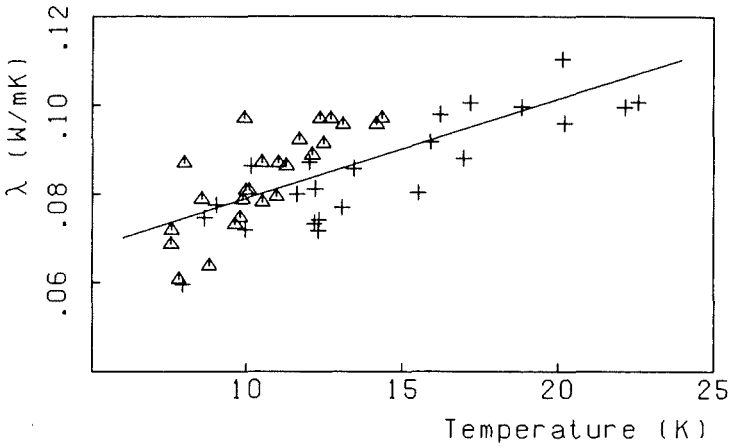

Fig.35: Measured thermal conductivity of insulating layers versus temperature: Δ, second test section; +, third test section

4. Conclusion

Pressure drop and transversal heat transfer are important parameters for a safe design of magnet systems with cable-in-conduit conductors. In the Helitex test facility of KfK/ITP first effort was made to investigate the pressure drop and the transversal heat transfer in the Wendelstein 7-X conductor.

The friction factor in the W7-X conductor is roughly three times the values in an equivalent smooth flow channel and can be well reproduced by a modified Prandtl-Karman equation.

To evaluate the experimental result concerning the transversal heat transfer, theoretical methods were developed which based on numerical analysis of two-dimensional heat conduction equation. The developed computer code THECON can be extended to any two-dimensional solution domain.

The experimental results show that the transversal heat transfer between the flow channel and the jacket can not be described accurately either by pure heat conduction or by pure heat convection. Based on a physical mechanism, a new model of transversal heat transfer was developed which considers heat conduction and heat convection simultaneously. By using the experimental results, equations were derived for the heat transfer between the jacket and helium as well as between the jacket and the strands in the W7-X superconductor.

Obviously, the transversal heat transfer coefficient in CICCs is dependent not only on the flow conditions, but also on the cabling structure. Therefore, it is necessary to measure the transversal heat transfer for every individual conductor used in fusion reactors. The theoretical method developed in the present work to evaluate the experimental results can be applied to any other CICCs.

The measured thermal conductivity of the insulating layer in two different test sections agrees well with each other. The thermal conductivity increases with increasing temperature. Additionally, it was found that the thermal resistance of the insulating layer is much higher than that between the flow channel and the jacket. Regarding the transversal heat transfer the thermal resistance of the jacket is negligble small.

Acknowledgements

The authors wish to express their thanks to R. Berggötz and H. Heckfuß for their help in performing the experiments in the Helitex test loop. The authors thank also the W7-X technical group of KfK and IPP for their support of this work.

References

[1] W. Maurer et.al
Development of the Superconducting Coils for the Modular Stellarator Wendelstein 7-X
Proc. of Jahrestagung Kerntechnik, Köln, May 25-27, 1993, INFORUM Verlags- und Verwaltungsgesellschaft mbH, Bonn, Germany.

[2] N. Mitchell for the ITER Team
Conductor Design for the ITER Toroidal and Poloidal Magnet Systems
MT13, Victoria, 1993.

[3] R.L. Wong
Program CICC, Flow and Heat Transfer in Cable-in-Conduit Conductors
Proceedings at the 13th Symp. on Fus. Eng., Knoxville, TN, October 1989 pp.1134-1137

[4] R. Meyder et.al
MAGS: A Computer Code System to Analyse the 3D Quench Propagation in Forced Flow Cooled Superconducting Magnet Systems
IAEA Technical Committee Meeting on 'Developments in Fusion Safety', June 1993, Toronto, Canada.

[5] L. Bottura, O.C. Zienkiewicz
Quench Analysis of Large Superconducting Magnets.
Part I: Model Description
Cryogenics, Vol 32 (1992), No 7, pp.659-667.

[6] D.W. Spitzer, Editor
Flow Measurement: Practical Guides for Measurement and Control
Instrument Society of American, 1991, printed in USA

[7] DIN: Deutsches Institut für Normung e.V.
Durchflußmessung mit Blenden, Düsen und Venturirohren in voll durchströmten Rohren mit Kreisquerschnitt
DIN-1952, Beuth Verlag GmbH, Berlin, Juli 1982

[8] B.A. Hands, V. Arp, R.D. McCarty
HEPROP-88: A Computer Code for Helium Properties
ICEC12, 460-463 (1988), Butterworths, Guildford, UK.

[9] H. Katheder
Optimum Thermohydraulic Operation Regime for Cable-in-Conduit Superconductors
Proceedings of the 15th International Cryogenics Engineering Conference, June 7-10, 1994, Genova, Italy, pp.594-598

[10] M. Sugimoto et.al
Test results of the DPC-TJ: thermal and hydraulic performance
Cryogenics (1993), Vol 33, No 6, pp.597-602

Appendix A: THECON - A computer code for two-dimensional heat conduction

Consider the problem of heat conduction in a two-dimensional (2D) domain. In steady state the temperature T satisfies a partial differential equation of elliptic type, as in the cartesian coordinate system with two space dimensions x and y:

$$\frac{\partial}{\partial x}\left(\lambda\frac{\partial T}{\partial x}\right)+\frac{\partial}{\partial y}\left(\lambda\frac{\partial T}{\partial y}\right)+q_v=0 \qquad \text{(A1)}$$

Numerical solution of the partial differential equation is not possible, even for simple domains. Finite difference method offers a powerful technique for the numerical solution of 2D heat conduction problems. A network of grid points, also called nodes, with grid spacing Δx and Δy is established throughout the domain of interest, as shown in figure A1.

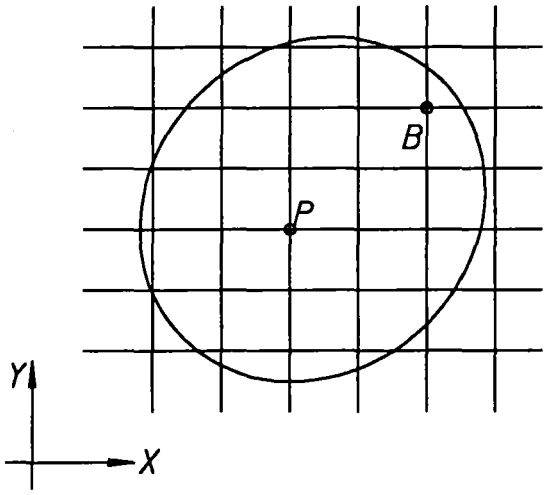

Figure A1: a two-dimensional domain with the network of grid points

Regarding the neighbourhood of a node considered we distinguish two types of nodes. The first type is called internal node, e.g. the point P in figure A1, whose four neighbouring grid points are inside of the solution domain, while for the other type called boundary node (point B in figure A1), at least one of its four neighbouring grid points are outside of the domain. The solution of equation (A1) is now considered to find out approximate values for the temperature at grid points. To this purpose finite difference equations must be provided for each one of the entire set of node points, i.e. of all internal nodes and all boundary nodes. The finite difference equations can be obtained either by replacing the governing partial differential equation in terms of partial difference quotients or by direct heat balance considerations which is used below.

A1. Finite difference equations for the internal nodes

Consider for clarity the cell control area around the point 0 in a 2D cartesian system with grid spacing Δx and Δy, as shown on figure A2, together with its four neighbouring nodes 1, 2, 3 and 4.

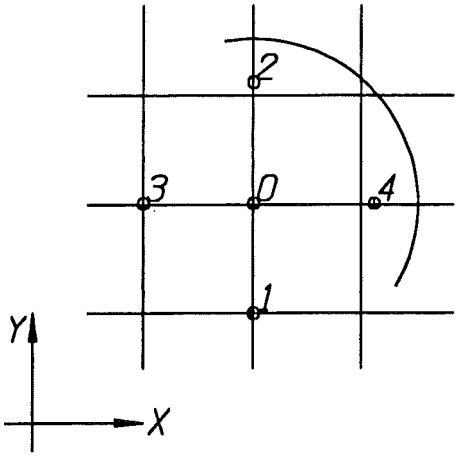

Figure A2: a internal node with its four neighbouring nodes

Using the central difference estimate we get the heat quantity transferred through the surface around the point 0

$$Q_{abcd} = \frac{\Delta y}{\Delta x}\lambda_{01}(T_0 - T_1) + \frac{\Delta y}{\Delta x}\lambda_{02}(T_0 - T_2) + \frac{\Delta x}{\Delta y}\lambda_{03}(T_0 - T_3) + \frac{\Delta x}{\Delta y}\lambda_{04}(T_0 - T_4) \qquad (A2)$$

Under steady-state conditions the energy balance for the control area a-b-c-d yields

$$\left(\sum_{i=1}^{4} A_i\right) T_0 - \left(\sum_{i=1}^{4} A_i T_i\right) = B \qquad (A3)$$

with

$$A_1 = \lambda_{01} / \Delta x^2 \qquad (A4)$$

$$A_2 = \lambda_{02} / \Delta x^2 \qquad (A5)$$

$$A_3 = \lambda_{03} / \Delta y^2 \qquad (A6)$$

$$A_4 = \lambda_{04} / \Delta y^2 \qquad (A7)$$

$$B = q_v \qquad (A8)$$

A2. Finite difference equations for the boundary nodes

To make the problem more comprehensible we restrict our consideration to a representative case, as shown in figure A3.

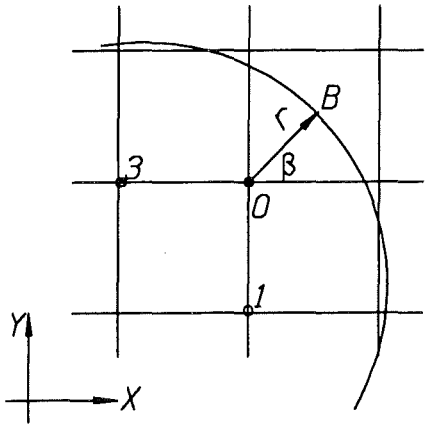

Figure A3: a boundary node with its neighbouring nodes

The neighbouring grid point 2 in the x-direction and grid point 4 in the y-direction are outside of the solution domain. The point B at the boundary surface satisfies that the line OB is perpendicular to the tangential line of the boundary curve at the point B. The angle between the x-coordinat and the line OB is β and the distance from the point O to the point B is r. If the boundary surface is described by a known function f(x,y)=0, the coordinates of the point B at the boundary surface can be obtained by solving the equations below:

$$f(x_B, y_B) = 0 \tag{A9}$$

$$\frac{\partial f}{\partial x}(y_B - y_0) - \frac{\partial f}{\partial y}(x_B - x_0) = 0 \tag{A10}$$

The distance r from O to B and the angle β are calculated by

$$r = \sqrt{(x_B - x_0)^2 + (y_B - y_0)^2} \tag{A11}$$

$$\sin(\beta) = \frac{x_0 - x_B}{r} \tag{A12}$$

In regard to heat transfer problem there are three different types of boundary conditions:

- Dirichlet boundary condition: Boundary surface temperature is known
- Neumann boundary condition: The normal gradient of temperature on boundary surface is known.
- Convective boundary condition: The boundary surface is in contact with fluid whose temperature Tf is known. Convective heat transfer takes place at the boundary surface, it applies:

$$q_B = \left(-\lambda \frac{\partial T}{\partial n}\right)_B = \alpha(T_B - T_f) \tag{A13}$$

where α is the heat transfer coeffitient.

Dirichlet boundary condition

The heat balance for the considered control cell yields

$$\frac{\lambda_{01}(T_0 - T_1)}{\Delta x(\Delta x/2 + \Delta x_1)} + \frac{\lambda_{02'}(T_0 - T_{2'})}{\Delta x_2(\Delta x/2 + \Delta x_1)} + \frac{k_{03}(T_0 - T_3)}{\Delta y(\Delta x/2 + \Delta y_1)} + \frac{k_{04'}(T_0 - T_{4'})}{\Delta y_2(\Delta x/2 + \Delta y_1)} = q_v \tag{A14}$$

This equation has the same form as that for internal nodes [eq.(2)].

$$A_0 T_0 - A_1 T_1 - A_3 T_3 = B \tag{A15}$$

with

$$A_1 = \frac{\lambda_{01}}{\Delta x(\Delta x/2 + \Delta x_1)} \tag{A16}$$

$$A_3 = \frac{\lambda_{03}}{\Delta y(\Delta y/2 + \Delta y_1)} \tag{A17}$$

$$A_0 = A_1 + A_3 + \frac{\lambda_{02'}}{\Delta x_2(\Delta x/2 + \Delta x_1)} + \frac{\lambda_{04'}}{\Delta y_2(\Delta y/2 + \Delta y_1)} \tag{A18}$$

$$B = q_v + T_B\left(\frac{\lambda_{02'}}{\Delta x_2(\Delta x/2 + \Delta x_1)} + \frac{\lambda_{04'}}{\Delta y_2(\Delta y/2 + \Delta y_1)}\right) \tag{A19}$$

Neumann boundary condition

The heat flux at the boundary node B is equal to

$$q_B = \lambda_{OB} \frac{T_O - T_B}{r} \tag{A20}$$

The temperature at the boundary point T_B can be computed approximately by extrapolating the temperature of the neighbouring grid points

$$T_B = T_0 + (T_0 - T_1)\frac{\Delta x_2}{\Delta x} + (T_0 - T_3)\frac{\Delta y_2}{\Delta y} \tag{A21}$$

Combining equation (A11) and equation (A12) yields

$$q_B = (T_1 - T_0)\frac{\lambda_{OB}}{r}\frac{\Delta x_2}{\Delta x} + (T_3 - T_0)\frac{\lambda_{OB}}{r}\frac{\Delta y_2}{\Delta y}$$

$$= (T_1 - T_0)\frac{\lambda_{OB}}{\Delta x}\cos\beta + (T_3 - T_0)\frac{\lambda_{OB}}{\Delta y}\sin\beta \qquad \text{(A22)}$$

For general cases the heat flux at the boundary point is computed by the following equation:

$$q_B = S_x \cdot (T_{ix} - T_0)\frac{\lambda_{OB}}{\Delta x}\cos\beta + S_y \cdot (T_{iy} - T_0)\frac{\lambda_{OB}}{\Delta y}\sin\beta \qquad \text{(A23)}$$

where ix and iy are the number of the neighbouring points in x- and in y-direction which locate inside of the solution domain. Both parameters S_x and S_y depend on the node number ix and iy. It applys

$$\begin{aligned} &S_x=1, \quad \text{if ix=1}, \quad S_x=-1, \quad \text{if ix=3} \\ &S_y=1, \quad \text{if iy=2}, \quad S_y=-1, \quad \text{if iy=4} \end{aligned} \qquad \text{(A24)}$$

The finite difference equation for boundary nodes with the Neumann boundary condition is

$$(A_{ix} + A_{iy})T_0 - A_{ix}T_{ix} - A_{iy}T_{iy} = B \qquad \text{(A25)}$$

with

$$A_{ix} = S_x\frac{\lambda_{OB}}{\Delta x}\cos\beta \qquad \text{(A26)}$$

$$A_{iy} = S_y\frac{\lambda_{OB}}{\Delta y}\sin\beta \qquad \text{(A27)}$$

$$B = q_B \qquad \text{(A28)}$$

Convective boundary condition

The heat flux from the boundary surface to fluid is determined either by equation (A8) or by equation (A11). Combining both equations we get

$$q_B = \frac{\lambda_{01}}{r}\frac{(T_o - T_f)}{1 + \frac{\lambda_{01}}{r \cdot \alpha}} \qquad \text{(A29)}$$

From equation (A14) and equation (A18) the finite different equation for boundary nodes with the convective boundary condition is obtained

$$A_0T_0 - A_{ix}T_{ix} - A_{iy}T_{iy} = B \qquad \text{(A30)}$$

with

$$A_0 = S_x\frac{\lambda_{OB}}{\Delta x}\cos\beta + S_y\frac{\lambda_{OB}}{\Delta y}\sin\beta + \frac{r \cdot a}{r \cdot a + \lambda_{OB}} \qquad \text{(A31)}$$

$$A_{ix} = S_x \frac{\lambda_{OB}}{\Delta x} \cos\beta \tag{A32}$$

$$A_{iy} = S_x \frac{\lambda_{OB}}{\Delta y} \sin\beta \tag{A33}$$

$$B = T_f \frac{r \cdot a}{r \cdot a + \lambda_{OB}} \tag{A34}$$

Appendix B: Test results of pressure drop

Parameters:

No.: test number
P: inlet pressure, bar
Tin: inlet temperature, K
m: mass flow, g/s
ΔP: pressure drop, mbar
Ren: Reynolds number, -
f: friction factor, eq.(5)

List of tables

Table B.1: Pressure drop in the first test section (dummy conductor)

Table B.2: Pressure drop in the first conductor of the second test section

Table B.3: Pressure drop in the second conductor of the second test section

Table B.4: Pressure drop in the first conductor of the third test section

Table B.5: Pressure drop in the second conductor of the third test section

Table B.1: Pressure drop in the first test section (dummy conductor)

No.	P (bar)	Tin (K)	m (g/s)	ΔP (mbar)	Ren	f
1	4.85	5.18	2.153	131.9	8142.7	0.0968
2	4.87	5.18	2.122	132.9	8802.0	0.0925
3	4.84	5.95	1.923	138.3	9671.6	0.0836
4	4.80	6.60	1.666	150.1	9068.3	0.0805
5	4.77	7.59	1.380	167.9	7335.0	0.0854
6	4.67	7.42	1.442	162.2	7945.2	0.0842
7	4..62	6.41	1.762	140.8	9539.4	0.0797
8	4.60	5.19	2.090	124.0	8039.9	0.0954
9	4.91	5.52	1.405	62.4	5622.1	0.1010
10	4.93	6.46	1.208	69.1	6348.7	0.0878
11	4.94	6.43	1.283	80.0	6798.0	0.0851
12	5.02	7.26	1.259	111.4	6734.3	0.0850
13	4.83	7.20	1.264	107.0	6913.0	0.0835
14	4.76	5.46	1.304	56.8	5211.9	0.1072
15	4.89	5.34	1.050	42.5	4062.7	0.1279
16	4.91	6.44	0.918	52.3	4842.4	0.1144
17	4.88	7.65	0.878	78.1	4702.9	0.1081
18	4.86	7.83	0.811	81.9	4200.0	0.1154
19	4.75	5.65	0.485	11.7	2013.2	0.1526
20	4.81	7.81	0.449	29.3	2327.3	0.1329
21	4.78	7.61	0.467	26.3	2527.5	0.1290
22	4.77	7.51	0.483	24.2	2652.7	0.1267
23	4.73	5.45	0.760	25.7	3031.1	0.1431
24	4.79	6.13	0.711	30.2	3664.8	0.1239
25	6.99	5.20	1.926	103.	6549.2	0.1010
26	7.03	5.20	1.919	104.	6962.6	0.0978
27	7.00	7.25	1.675	120.	7827.2	0.0886
28	6.88	5.23	1.413	63.4	5297.3	0.1068
29	6.65	6.91	1.334	77.7	6210.1	0.0973
30	6.61	5.25	1.114	45.1	4178.9	0.1228
31	6.50	6.82	1.051	55.7	4879.0	0.1157
32	6.62	7.34	0.774	39.1	3741.6	0.1172
33	5.98	6.41	0.759	39.1	3718.9	0.1173
34	6.11	6.94	0.459	17.4	2272.0	0.1428
35	5.60	6.83	0.459	15.7	2318.1	0.1388
36	3.23	5.28	1.022	39.2	4512.9	0.1116
37	3.25	6.38	0.534	46.3	3182.5	0.1258
38	3.19	5.60	0.731	31.9	4307.4	0.1102
39	3.19	5.40	0.493	13.3	2295.9	0.1515
40	3.20	5.83	0.426	21.2	2649.4	0.1252

Table B.1: Pressure drop in the first test section (dummy conductor) (continued)

No.	P (bar)	Tin (K)	m (g/s)	ΔP (mbar)	Ren	f
41	3.19	7.45	0.413	31.0	2543.1	0.1288
42	3.35	5.12	2.218	152.0	9292.4	0.0979
43	2.88	5.42	0.518	16.3	2646.8	0.1510
44	2.88	5.43	0.505	15.7	2606.8	0.1504
45	3.01	6.04	0.252	10.4	1643.7	0.1833
46	3.09	6.45	0.221	13.1	1322.5	0.1953
47	3.05	7.88	0.200	14.4	1115.1	0.1933
48	3.11	9.19	0.185	15.3	1036.2	0.2212
49	3.11	6.01	0.327	14.0	2085.5	0.1614
50	3.18	6.11	0.303	16.6	1892.5	0.1681
51	3.20	8.56	0.312	31.7	1669.6	0.1641
52	5.55	5.72	0.389	10.9	1541.6	0.2279
53	5.55	8.01	0.296	12.1	1538.9	0.1777
54	5.54	8.21	0.297	14.6	1481.1	0.1705
55	5.07	5.27	1.725	86.3	6531.5	0.0981
56	5.18	5.27	1.716	88.8	7087.6	0.0942
57	5.15	6.21	1.539	94.1	7689.5	0.0865
58	5.08	5.54	0.748	25.2	2960.1	0.1451
59	5.07	6.06	0.722	29.2	3623.3	0.1201
60	5.06	5.89	0.322	11.4	1644.1	0.1814

Table B.2: Pressure drop in the first conductor of the second test section

No.	P (bar)	T (K)	m (g/s)	ΔP (mbar)	Ren	f
1	5.26	9.75	1.055	152.1	5242.7	0.0988
2	4.69	5.27	1.566	78.0	6012.5	0.0916
3	4.71	5.22	2.022	122.0	7688.6	0.0868
4	4.66	5.30	1.269	53.5	4910.1	0.0950
5	4.60	5.45	0.854	26.3	3421.3	0.0994
6	4.64	5.34	1.127	45.1	4398.9	0.1006
7	4.72	9.04	1.100	169.4	5752.9	0.1004
8	3.00	5.29	1.039	44.0	4711.7	0.1015
9	4.01	5.29	2.301	149.5	9330.8	0.0779
10	4.18	5.23	2.990	233.5	11823.1	0.0738
11	4.29	5.21	3.323	280.5	12968.9	0.0726
12	3.09	5.14	1.833	102.4	7815.7	0.0816
13	3.09	5.14	1.834	102.6	7802.2	0.0819
14	3.16	7.13	1.107	146.8	6898.9	0.0798
15	3.09	5.14	1.834	102.7	7807.2	0.0819
16	3.09	5.14	1.746	102.7	7444.3	0.0901

Table B.3: Pressure drop in the second conductor of the second test section

No.	P (bar)	T (K)	m (g/s)	ΔP (mbar)	Ren	f
1	4.74	5.33	1.370	85.5	5301.4	.1300
2	4.76	5.27	1.743	129.5	6663.6	.1232
3	4.71	5.37	1.126	61.3	4404.3	.1364
4	4.66	5.45	.974	48.2	3881.4	.1406
5	4.67	5.50	.621	29.2	2501.4	.2070
6	4.67	5.42	.578	24.8	2289.0	.2066
7	4.82	14.74	.524	145.4	2151.6	.2028
8	4.76	5.25	1.059	61.2	4032.8	.1582
9	4.68	5.41	.590	26.0	2328.2	.2085
10	3.06	5.35	1.020	55.6	4712.4	.1298
11	4.28	5.31	2.465	310.0	9817.5	.1426
12	4.26	5.30	2.311	260.0	9205.8	.1361
13	4.26	5.30	2.201	230.5	8767.4	.1330
14	3.09	5.23	1.307	82.1	5723.6	.1247
15	3.09	5.22	1.308	82.2	5714.6	.1250
16	3.14	5.32	1.340	88.4	6036.5	.1231
17	3.10	5.23	1.310	82.3	5726.4	.1248
18	3.10	5.23	1.350	86.6	5897.3	.1236

Table B.4: Pressure drop in the first conductor of the third test section

No.	P (bar)	T (K)	m (g/s)	ΔP (mbar)	Ren	f
1	2.93	5.44	1.428	96.4	7266.7	.1002
2	2.89	5.42	1.501	104.3	7573.5	.0997
3	3.00	5.44	1.763	134.4	8684.2	.0960
4	5.20	5.46	2.414	194.5	9285.5	:0949
5	3.70	5.47	1.705	113.0	7467.1	.0987
6	3.79	5.52	1.316	73.5	5793.6	.1066
7	3.77	5.56	1.073	53.1	4813.4	.1129
8	3.74	5.63	.870	37.8	4018.2	.1173
9	3.74	5.59	.961	44.2	4368.0	.1153
10	2.98	5.39	.988	47.5	4745.2	.1123
11	2.98	5.42	.793	33.5	3884.4	.1193
12	2.97	5.44	.686	26.6	3439.1	.1224
13	2.97	5.46	.587	20.9	2970.3	.1292
14	2.97	5.48	.496	16.3	2573.8	.1351
15	2.97	5.52	.393	11.6	2109.6	.1443
16	2.97	5.54	.398	11.5	2180.8	.1331
17	2.69	5.43	.415	12.8	2399.3	.1265
18	2.73	10.58	.282	44.3	1463.5	.1748
19	3.96	6.99	1.752	315.8	10240.6	.0998
20	3.90	8.29	1.227	242.1	6896.1	.1060
21	3.67	5.30	1.603	98.4	6720.3	.1026
22	3.68	5.27	2.048	150.9	8502.6	.0975
23	3.68	5.24	2.378	195.1	9800.7	.0943
24	3.80	5.26	2.724	248.2	11163.2	.0917
25	3.75	5.24	3.078	312.5	12620.7	.0905
26	3.84	5.23	3.311	354.3	13412.2	.0896

Table B.5: Pressure drop in the second conductor of the third test section

No.	P (bar)	T (K)	m (g/s)	ΔP (mbar)	Ren	f
1	3.00	5.47	1.199	86.0	6046.7	.1280
2	3.06	5.43	1.632	157.4	7851.4	.1355
3	5.27	5.46	2.093	177.2	8015.3	.1154
4	3.78	5.50	1.516	103.1	6653.3	.1132
5	3.87	5.55	1.192	65.4	5256.3	.1150
6	3.85	5.60	.972	46.0	4369.6	.1186
7	3.84	5.59	1.011	49.0	4530.2	.1173
8	3.83	5.59	.994	47.5	4454.4	.1178
9	3.07	5.42	.670	29.0	3210.4	.1488
10	3.06	5.42	.542	20.8	2598.0	.1633
11	3.07	5.40	.607	24.5	2874.5	.1563
12	3.07	5.42	.516	19.5	2464.2	.1697
13	3.06	5.44	.433	15.3	2107.8	.1840
14	3.06	5.49	.356	11.0	1788.0	.1867
15	3.05	5.53	.291	8.2	1516.6	.1950
16	3.08	9.20	.260	30.0	1445.4	.1896
17	2.78	5.42	.346	11.3	1855.7	.1850
18	2.79	9.95	.227	29.1	1221.6	.1946
19	4.02	7.60	1.446	297.0	8307.5	.1153
20	3.97	9.31	1.032	230.9	5500.0	.1212
21	3.73	5.37	1.351	81.3	5735.0	.1175
22	3.80	5.30	1.941	171.1	8031.4	.1231
23	3.82	5.27	2.177	223.0	8930.5	.1288
24	4.02	5.27	2.670	327.5	10774.0	.1274
25	3.71	5.30	2.151	221.1	8967.6	.1288
26	3.71	5.29	2.085	204.1	8672.7	.1269

Appendix C: Test results of transversal heat transfer between the flow channel and the jacket

Parameters:

No.: test number
P: inlet pressure, bar
m: mass flow, g/s
Q: heating power, W
Tin: inlet temperature, K
Tex: outlet temperature, K
Tcu: temperature of the heating block, K

Table C: Test results of transversal heat transfer between the flow channel and the jacket

No.	P (bar)	m (g/s)	Q (W)	Tin (K)	Tex (K)	Tcu (K)
1	3.071	1.143	0.00	5.175	5.159	5.142
2	2.784	1.047	24.84	5.151	6.302	9.980
3	2.847	1.048	25.54	5.534	7.268	10.610
4	2.912	1.115	25.62	5.735	8.190	11.190
5	3.010	1.304	25.58	6.245	8.816	11.660
6	2.768	1.434	2.10	5.05?	5.186	5.557
7	2.765	1.392	5.33	5.059	5.368	6.193
8	2.772	1.343	5.25	5.271	5.432	6.269
9	2.786	1.149	5.18	5.524	5.593	6.487
10	2.805	1.126	5.22	5.644	5.865	6.748
11	2.873	1.102	5.21	6.175	6.680	7.452
12	2.997	1.441	5.21	7.039	7.578	8.268
13	2.829	0.803	5.24	5.196	5.513	6.401
14	2.851	0.746	5.23	5.478	5.629	6.563
15	2.896	0.670	5.22	5.750	6.315	7.148
16	3.001	0.710	3.82	6.610	7.314	7.827
17	2.854	0.857	12.74	5.225	5.780	7.904
18	2.887	0.802	12.83	5.463	6.075	8.122
19	3.006	0.643	12.79	6.034	8.411	9.823
20	3.176	2.054	21.45	5.561	5.862	8.963
21	3.141	2.101	14.24	5.545	5.695	7.797
22	3.131	2.159	4.86	5.532	5.576	6.376
23	2.970	1.105	20.32	5.395	6.245	9.466
24	2.941	1.144	14.26	5.374	5.794	8.296
25	2.943	1.197	7.09	5.363	5.579	6.918
26	3.369	0.679	5.18	5.676	5.986	6.968
27	3.232	0.656	12.36	5.630	6.717	8.597
28	2.944	0.420	5.12	5.605	6.245	7.182
29	2.911	0.810	10.06	5.476	5.872	7.654
30	3.372	1.844	14.11	5.253	5.745	7.753
31	3.444	1.337	13.88	5.394	5.937	8.049
32	3.307	1.621	25.99	5.120	6.000	9.655
33	3.266	1.716	10.29	5.112	5.623	7.159
34	3.304	1.619	7.43	5.638	5.772	6.956
35	3.342	1.461	7.45	5.970	6.251	7.431
36	3.399	1.185	7.47	7.310	8.163	9.108
37	3.226	0.927	18.41	5.284	6.342	9.104
38	3.169	0.351	8.45	5.592	7.356	8.455
39	3.147	0.408	2.66	5.552	5.817	6.378
40	3.072	0.360	3.48	6.561	7.772	8.129

Table C: Test results of transversal heat transfer between the flow channel and the jacket (continued)

No.	P (bar)	m (g/s)	Q (W)	Tin (K)	Tex (K)	Tcu (K)
41	3.268	2.034	8.12	5.760	5.838	7.040
42	3.284	1.313	8.52	6.938	7.745	8.850
43	7.056	1.777	12.71	5.325	6.486	7.883
44	6.988	1.784	6.14	5.323	5.978	6.727
45	7.102	1.641	6.08	7.227	7.569	8.204
46	7.048	1.483	25.81	5.251	7.477	10.160
47	4.852	2.153	0.00	5.182	5.174	5.121
48	4.873	2.122	13.62	5.183	6.020	7.606
49	4.855	2.055	26.00	5.193	6.476	9.458
50	4.836	1.923	25.26	5.948	6.887	9.890
51	4.798	1.666	25.68	6.597	7.951	10.800
52	4.774	1.380	25.31	7.585	10.070	12.410
53	4.670	1.442	12.31	7.418	8.448	9.841
54	4.619	1.762	12.34	6.406	6.868	8.444
55	4.596	2.090	0.00	5.187	5.203	5.253
56	4.914	1.405	0.00	5.521	5.517	5.536
57	4.907	1.360	10.71	5.528	6.373	7.711
58	4.925	1.208	10.77	6.463	7.150	8.487
59	4.938	1.283	18.59	6.426	7.628	9.798
60	5.022	1.259	18.27	7.256	8.990	10.835
61	4.828	1.264	10.01	7.204	8.102	9.240
62	4.759	1.304	0.00	5.459	5.477	5.454
63	4.825	1.304	9.91	5.368	6.273	7.524
64	4.889	1.050	0.00	5.339	5.358	5.319
65	4.907	1.021	10.15	5.341	6.404	7.668
66	4.912	0.918	10.16	6.441	7.228	8.481
67	4.881	0.878	10.23	7.648	9.101	10.100
68	4.862	0.811	17.89	7.826	10.830	12.290
69	4.746	0.485	0.00	5.648	5.710	5.661
70	4.810	0.484	3.63	5.660	6.465	6.921
71	4.823	0.471	10.02	5.690	7.618	8.777
72	4.807	0.449	10.08	7.805	11.090	11.810
73	4.776	0.467	4.36	7.612	8.938	9.332
74	4.770	0.483	0.00	7.506	7.541	7.454
75	4.732	0.760	0.00	5.445	5.471	5.419
76	4.786	0.711	8.82	6.133	7.042	8.166
77	6.987	1.926	0.00	5.200	5.212	5.176
78	7.025	1.919	9.49	5.204	6.131	7.209
79	6.981	1.799	34.56	5.228	7.635	11.085
80	7.004	1.675	12.73	7.250	8.001	9.341

Table C: Test results of transversal heat transfer between the flow channel and the jacket (continued)

No.	P (bar)	m (g/s)	Q (W)	Tin (K)	Tex (K)	Tcu (K)
81	6.879	1.413	9.85	5.230	6.424	7.514
82	6.649	1.334	9.78	6.905	7.601	8.639
83	6.612	1.114	6.49	5.247	6.257	6.994
84	6.502	1.051	6.55	6.816	7.382	8.066
85	6.683	0.807	9.68	5.363	7.041	8.089
86	6.622	0.774	9.61	7.337	8.600	9.522
87	5.980	0.759	25.37	6.413	9.936	12.145
88	6.572	0.468	9.22	5.649	7.896	8.837
89	6.105	0.459	9.19	6.935	9.056	9.869
90	5.602	0.460	3.63	6.828	7.612	7.991
91	3.242	2.206	10.27	5.556	5.669	6.923
92	3.293	2.028	10.18	5.805	5.916	7.255
93	3.426	2.148	10.12	6.095	6.307	7.610
94	3.454	2.087	18.79	6.158	6.819	9.064
95	3.260	1.407	10.12	5.314	5.764	7.470
96	3.274	1.374	10.05	5.492	5.830	7.488
97	3.303	1.316	17.40	5.511	6.135	8.767
98	3.306	1.274	26.06	5.332	6.578	10.170
99	3.227	1.022	0.00	5.278	5.324	5.424
100	3.253	0.986	9.86	5.249	5.833	7.377
101	3.254	0.934	17.56	5.246	6.305	8.900
102	3.262	0.857	25.36	5.259	7.423	10.585
103	3.246	0.534	13.49	6.375	9.860	11.090
104	3.189	0.731	7.25	5.600	5.988	7.248
105	3.222	0.731	11.92	5.463	6.281	8.142
106	3.191	0.493	0.00	5.402	5.459	5.477
107	3.199	0.478	6.29	5.429	6.066	7.091
108	3.207	0.444	13.52	5.458	7.994	9.507
109	3.200	0.426	10.03	5.826	8.279	9.354
110	3.220	0.375	9.27	8.296	12.260	12.815
111	3.193	0.413	0.00	7.445	7.547	7.495
112	3.349	2.218	0.00	5.123	5.105	5.120
113	2.883	0.518	0.00	5.418	5.411	5.398
114	2.878	0.505	0.00	5.426	5.418	5.403
115	3.005	0.252	0.00	6.040	6.051	6.008
116	3.089	0.221	5.46	6.447	9.561	9.990
117	3.108	0.280	10.14	8.803	15.070	15.360
118	3.046	0.201	3.85	7.881	10.410	10.890
119	3.110	0.185	0.00	9.186	9.293	9.231
120	3.114	0.327	0.00	6.013	6.034	6.019

Table C: Test results of transversal heat transfer between the flow channel and the jacket (continued)

No.	P	m	Q	Tin	Tex	Tcu
	(bar)	(g/s)	(W)	(K)	(K)	(K)
121	3.178	0.303	5.52	6.108	8.257	8.814
122	3.206	0.307	12.05	6.656	12.760	13.430
123	3.224	0.353	12.05	8.354	13.290	14.160
124	3.196	0.313	5.56	8.562	11.260	11.650
125	5.554	0.389	0.00	5.718	5.781	5.751
126	5.545	0.386	6.26	5.791	7.385	8.080
127	5.543	0.381	11.76	5.838	9.034	10.110
128	5.546	0.296	0.00	8.006	8.079	8.015
129	5.541	0.297	6.01	8.207	11.000	11.390
130	5.545	0.328	11.90	8.928	14.640	15.135
131	5.066	1.725	0.00	5.271	5.265	5.217
132	5.178	1.716	11.62	5.269	6.158	7.471
133	5.166	1.639	23.10	5.283	6.735	9.360
134	5.194	1.548	36.15	5.312	7.545	11.480
135	5.153	1.539	17.39	6.208	7.085	9.172
136	5.081	0.748	0.00	5.536	5.583	5.599
137	5.084	0.732	9.93	5.402	6.754	8.000
138	5.088	0.723	17.93	5.365	7.672	9.797
139	5.073	0.722	11.57	6.055	7.404	8.848
140	5.033	0.368	0.00	5.622	5.757	5.789
141	5.067	0.369	5.46	5.730	7.163	7.834
142	5.063	0.322	11.58	5.885	9.789	10.750
143	5.049	0.324	5.27	6.152	7.646	8.281

Appendix D: Test results of thermal conductivity of insulating layers

Parameters:

No.: test number
T11: temperature at the inlet of the first conductor, K
T12: temperature in the middle of the first conductor, K
T13: temperature at the outlet of the first conductor, K
P1: pressure at the inlet of the first conductor, bar
m1: mass flow through the first conductor, g/s
T21: temperature at the inlet of the second conductor, K
T22: temperature in the middle of the second conductor, K
T23: temperature at the outlet of the second conductor, K
P2: pressure at the inlet of the second conductor, bar
m2: mass flow through the second conductor, g/s

List of tables

Table D.1: Measured data of the second test section

Table D.2: Measured data of the third test section

Table D.3: Evaluated results of the second test section

Table D.4: Evaluated results of the third test section

Table D.1: Measured results in the second test section

No.	T11 (K)	T12 (K)	T13 (K)	P1 (bar)	m1 (g/s)	T21 (K)	T22 (K)	T23 (K)	P2 (bar)	m2 (g/s)
1	9.98	9.96	9.52	5.25	1.10	5.48	5.78	6.12	5.18	1.03
2	15.30	14.35	13.24	5.27	0.99	5.47	6.14	6.61	5.13	1.03
3	17.93	16.68	15.25	5.40	1.09	5.46	6.28	6.83	5.17	1.08
4	18.00	16.70	15.21	5.44	1.07	5.25	5.80	6.22	5.41	2.08
5	15.28	14.33	13.19	5.34	1.02	5.23	5.65	6.02	5.40	2.09
6	14.99	14.48	13.73	5.69	1.91	5.30	5.69	6.07	5.20	2.01
7	15.09	14.56	13.83	5.02	1.02	9.34	9.60	10.31	5.00	1.01
8	19.25	18.97	18.37	5.14	0.99	16.24	16.28	17.21	5.22	0.94
9	10.15	10.89	11.17	5.09	0.99	14.59	13.81	13.75	5.32	0.99
10	10.25	11.47	12.15	5.08	0.97	18.68	17.15	16.90	5.48	1.04
11	9.87	10.69	11.03	5.08	1.01	15.46	14.07	13.96	5.16	0.62
12	9.95	10.77	11.13	5.16	0.98	15.31	14.25	14.19	5.36	0.76
13	5.16	5.22	5.17	5.06	2.70	5.23	5.14	5.21	5.12	2.14
14	5.26	5.30	5.27	4.69	1.64	5.33	5.25	5.32	4.74	1.33
15	5.21	5.25	5.23	4.71	2.12	5.27	5.20	5.27	4.76	1.69
16	5.30	5.34	5.30	4.66	1.33	5.39	5.30	5.36	4.71	1.09
17	5.45	5.50	5.45	4.60	0.90	5.46	5.38	5.45	4.66	0.94
18	5.43	5.49	5.44	4.61	0.73	5.51	5.42	5.50	4.67	0.65
19	5.62	5.65	5.58	4.59	0.63	5.40	5.34	5.45	4.67	0.61
20	10.41	10.13	9.48	4.64	0.70	5.41	5.89	6.25	4.63	0.60
21	14.59	13.63	12.38	4.72	0.79	5.42	6.21	6.76	4.64	0.60
22	5.56	5.97	6.13	4.57	0.70	9.89	9.04	8.83	4.73	0.63
23	5.57	6.31	6.65	4.60	0.70	14.75	12.78	12.02	4.81	0.59
24	8.83	9.92	10.42	4.70	0.72	15.15	13.61	13.33	4.83	0.57
25	11.18	12.11	12.39	4.71	0.69	15.31	14.10	14.17	4.82	0.55
26	5.34	5.37	5.33	4.64	1.18	5.24	5.17	5.26	4.76	1.03
27	5.70	5.71	5.60	4.60	0.45	5.38	5.33	5.44	4.68	0.62
28	5.50	5.95	6.09	4.60	0.72	10.65	9.08	8.47	4.65	0.30
29	7.30	7.86	7.99	4.62	0.65	11.12	9.80	9.44	4.64	0.28
30	9.16	9.24	8.92	4.71	1.16	5.79	6.28	6.75	4.56	0.28
31	14.54	13.85	13.01	4.79	1.01	5.82	7.20	9.04	4.56	0.28
32	14.68	14.40	13.90	4.82	1.00	9.60	11.09	12.48	4.60	0.27
33	5.28	5.32	5.29	3.00	1.09	5.36	5.27	5.34	3.06	0.99
34	9.18	9.03	8.61	3.32	1.12	5.38	5.44	5.59	3.17	1.06
35	7.33	7.85	8.01	3.19	.01	11.11	10.33	10.25	3.36	0.86
36	7.01	7.71	8.12	3.25	.15	14.45	13.07	12.83	3.64	1.01
37	18.24	16.95	15.98	3.20	.73	7.62	11.65	14.08	2.96	0.23
38	5.29	5.33	5.29	4.00	2.42	5.32	5.24	5.30	4.28	2.39
39	5.23	5.28	5.23	4.17	3.14	5.31	5.23	5.29	4.26	2.24
40	5.21	5.25	5.21	4.29	3.49	5.31	5.23	5.29	4.26	2.14

Table D.1: Measured results in the second test section (continued)

No.	T11 (K)	T12 (K)	T13 (K)	P1 (bar)	m1 (g/s)	T21 (K)	T22 (K)	T23 (K)	P2 (bar)	m2 (g/s)
41	5.14	5.18	5.14	3.09	1.93	5.24	5.16	5.22	3.09	1.27
42	5.13	5.17	5.14	3.09	1.93	5.23	5.15	5.21	3.09	1.27
43	7.21	7.30?	7.05	3.16	1.16	5.24	5.26	5.39	3.14	1.30
44	5.14	5.17	5.14	3.09	1.93	5.24	5.16	5.22	3.10	1.27
45	11.54	10.83	9.93	3.15	0.91	5.24	5.39	5.55	3.13	1.32
46	5.14	5.18	5.14	3.09	1.84	5.24	5.15	5.21	3.10	1.31
47	9.07	8.88	8.40	3.12	0.98	5.24	5.31	5.46	3.11	1.33
48	13.89	12.67	11.78	3.17	0.90	5.58	6.55	8.22	3.03	0.29
49	10.72	9.84	9.08	3.09	0.44	5.55	5.87	6.54	3.08	0.28
50	17.35	14.37	12.92	3.10	0.39	5.56	7.52	9.71	3.06	0.27
51	12.17	11.35	10.58	3.21	0.89	5.65	5.69	5.90	3.12	0.86

Table D.2: Measured results in the third test section

No.	T11 (K)	T12 (K)	T13 (K)	P1 (bar)	m1 (g/s)	T21 (K)	T22 (K)	T23 (K)	P2 (bar)	m2 (g/s)
1	9.17	9.06	8.70	3.82	.81	5.55	5.61	5.76	3.91	1.02
2	12.25	11.79	11.16	3.92	.86	5.52	5.66	5.85	3.95	1.14
3	50.00	18.70	17.05	4.06	.83	5.52	5.84	6.11	3.96	1.19
4	12.85	12.44	11.83	4.14	1.10	5.57	5.74	5.95	4.00	1.01
5	5.34	5.59	5.60	3.06	1.15	15.32	14.07	13.82	3.69	.98
6	5.35	5.67	5.75	3.04	1.12	20.62	18.45	17.94	3.80	.93
7	7.63	8.57	9.18	3.20	.98	19.73	17.94	17.73	3.82	.95
8	7.58	9.05	10.15	3.19	1.00	25.76	22.83	50.00	3.91	.90
9	7.59	9.27	10.54	3.20	1.01	27.98	24.68	50.00	4.02	.93
10	12.68	14.41	15.42	3.39	.96	28.07	25.17	50.00	4.04	.92
11	16.20	17.85	18.37	3.46	.90	28.23	25.64	50.00	4.05	.92
12	50.00	22.25	50.00	3.53	.85	28.06	25.98	50.00	4.05	.90
13	19.03	17.68	16.19	3.23	.83	8.06	8.27	8.35	3.02	.91
14	11.36	11.05	10.62	5.36	.98	5.72	5.92	6.20	5.39	.96
15	14.98	14.36	13.55	5.57	1.01	5.70	6.09	6.48	5.51	.97
16	5.61	6.05	6.26	5.64	1.17	13.47	12.66	12.65	6.08	1.12
17	5.61	6.38	6.70	5.44	1.20	21.17	19.30	19.10	6.11	1.10
18	5.62	6.75	7.37	5.33	1.16	30.02	26.63	50.00	6.18	1.04
19	9.54	11.13	12.21	5.43	1.06	28.83	25.82	50.00	6.15	1.06
20	15.75	17.38	18.11	5.56	.96	29.58	26.96	50.00	6.17	1.02
21	5.65	6.03	6.16	5.18	1.52	14.59	13.81	13.90	6.57	2.14
22	5.65	5.94	6.05	5.32	1.65	12.66	11.99	12.20	6.89	2.46
23	5.63	6.08	6.24	4.97	1.69	17.86	16.97	17.13	6.14	1.71
24	12.37	12.16	11.66	5.55	1.67	5.61	5.69	5.90	5.40	2.12
25	9.64	9.69	9.50	3.04	.41	9.06	9.02	9.33	3.18	.26
26	6.08	6.55	6.72	6.13	.52	10.56	9.81	9.69	6.35	.41
27	6.13	7.26	7.93	5.91	.51	18.57	15.91	15.07	6.16	.39
28	5.49	5.68	5.69	3.03	.49	11.12	9.97	9.55	3.27	.36
29	5.48	6.03	6.83	3.00	.50	21.37	17.15	16.04	3.32	.37
30	5.50	6.91	8.76	3.01	.49	29.60	23.08	50.00	3.39	.37
31	10.35	14.26	16.12	3.12	.45	31.80	25.42	50.00	3.41	.35
32	18.16	21.90	50.00	3.20	.43	34.31	28.32	50.00	3.41	.33
33	50.00	24.14	50.00	3.55	.48	31.68	28.16	50.00	3.76	.38
34	50.00	18.39	16.26	3.17	.56	5.50	6.20	7.70	3.16	.38
35	50.00	19.33	17.94	3.21	.56	10.69	12.54	14.27	3.25	.33
36	7.07	7.06	6.92	3.96	1.96	7.67	7.47	7.52	4.12	1.45
37	8.32	8.38	8.26	3.90	1.37	9.37	9.09	9.24	4.07	1.03
38	5.27	5.49	5.53	3.88	2.41	12.32	11.67	11.66	4.76	1.68
39	5.31	5.56	5.63	3.76	2.30	14.32	13.53	13.56	5.31	2.03
40	5.40	5.69	5.68	3.37	2.22	19.82	18.51	18.61	5.73	2.05

Table D.2: Measured results in the third test section (continued)

No.	T11 (K)	T12 (K)	T13 (K)	P1 (bar)	m1 (g/s)	T21 (K)	T22 (K)	T23 (K)	P2 (bar)	m2 (g/s)
41	10.06	10.40	10.50	4.29	2.35	19.51	18.38	18.66	5.74	2.04
42	9.24	9.21	8.97	4.41	2.66	10.95	10.50	10.53	5.13	2.22
43	9.68	9.60	9.31	4.70	2.94	10.17	9.79	9.83	4.99	2.18
44	10.32	10.13	9.73	5.35	3.50	8.62	8.38	8.45	4.82	2.18
45	8.80	8.65	8.23	5.19	3.83	8.82	8.54	8.58	4.46	1.92

Table D.3: Thermal conductivity of the insulating layer of the second test section

No.	T (K)	λ (W/m K)
1	10.10	0.0809
2	11.29	0.0864
3	11.04	0.0870
4	9.89	0.0787
5	9.99	0.0809
6	12.11	0.0888
7	14.35	0.0971
8	12.37	0.0969
9	12.46	0.0913
10	9.80	0.0747
11	7.60	0.0719
12	9.65	0.0731
13	11.72	0.0922
14	13.11	0.0956
15	7.59	0.0687
16	8.82	0.0638
17	10.53	0.0781
18	12.71	0.0969
19	10.50	0.0871
20	14.18	0.0957
21	8.01	0.0870
22	9.96	0.0971
23	7.85	0.0607
24	10.98	0.0794
25	8.57	0.0788

Parameters:

No.: Test number
T: Average temperature
λ: Thermal conductivity

Table D.4: Thermal conductivity of the insulating layer of the third test section

No.	T (K)	λ (W/m K)
1	8,67	0.0746
2	12.02	0.0872
3	9.05	0.0775
4	9.97	0.072
5	12.21	0.0812
6	13.45	0.0858
7	16.24	0.0980
8	17-20	0.1005
9	20.15	0.1104
10	22.14	0.0995
11	10.16	0.0863
12	12.02	0.0872
13	16.98	0.0881
14	18.85	0.996
15	22.58	0.1007
16	11.63	0.0800
17	7.97	0.0596
18	12.18	0.0733
19	15.51	0.0803
20	20.24	0.0960
21	12.33	0.0741
22	15.92	0.0918
23	12.31	0.0717

Parameters:

No.: Test number
T: Average temperature
λ: Thermal conductivity